Processing of a Mullite Matrix, Molybdenum Disilicide Reinforced Composite

by

Richard Brynsvold

A thesis submitted in partial fulfillment
of the requirements for the degree of

Master of Science
in
Materials Science and Engineering

University of Washington

1991

Approved by _____
(Chairperson of Supervisory Committee)

Program Authorized
to Offer Degree Materials Science and Engineering

Date December 11, 1991

In presenting this thesis in partial fulfillment of the requirements for a Master's degree at the University of Washington, I agree that the Library shall make its copies freely available for inspection. I further agree that extensive copying of this thesis is allowable only for scholarly purposes, consistent with "fair use" as prescribed in the U.S. Copyright Law. Any other reproduction for any purposes or by any means shall not be allowed without my written permission.

Signature Richard A Reynolds

Date 11 December 1991

Statement A per telecon
Maj. Jill Whisker TAPC-OPB-D
Alexandria, VA 22332-0411

NWW 1/22/92

University of Washington
Abstract

Processing of a Mullite Matrix, Molybdenum Disilicide Reinforced Composite for Potential High Temperature Use

by
Richard Alan Brynsvold

Chairperson of the Supervisory Committee: Professor Ilhan A. Aksay
Department of Materials Science and Engineering

A mullite matrix reinforced with $MoSi_2$ particles was investigated as a potential high temperature composite material. Mullite is well known for its high temperature strength, creep resistance, corrosion resistance and ability to withstand oxidizing environments. $MoSi_2$ has the potential to be a good reinforcement because: it forms a protective silica layer during oxidation, undergoes a brittle to ductile transformation at 900-1000°C which would increase high temperature composite toughness, and is thermodynamically stable with mullite. Samples containing 2.5 to 20 vol% $MoSi_2$ were processed using both hot pressing and pressureless sintering techniques. Low temperature mechanical testing was performed both in the as sintered state and after oxidation at 1400°C for 96 hours. Densities of greater than 93% of theoretical were attained for composites containing up to 20 vol% $MoSi_2$ via pressureless sintering. K_{Ic} and strength values of the as-sintered composite were up to two times that of monolithic mullite. After oxidation at 1400°C for 96 hours, strength improved by 1.5 times over the as-sintered strength, and fracture toughness improved by 2.5 times over the as-sintered toughness indicating that the composite is self-healing during oxidation.

TABLE OF CONTENTS

LIST OF FIGURES

LIST OF TABLES

ACKNOWLEDGMENTS

The author wishes to express sincere appreciation to Professor Ilhan Aksay for his guidance and support throughout this research. In addition, appreciation to: Dave Milius for his direction and expertise in use of the ACML laboratory equipment, and Jim Webb for providing his processing route to form the matrix of the composite. Finally, a special thanks for the constant understanding and support received from Tina and Douglas throughout my graduate education and research.

CHAPTER 1
INTRODUCTION

Ceramics have long been used for many applications: pottery, cookware, art, refractories, and structural materials to name a few. The reasons for these widespread uses are because of key properties of ceramics, i.e. their formability, strength, stability at high temperatures, low density, resistance to wear and corrosion, and that the "natural ingredients" for ceramics are abundant and therefore cheap. But until recently, ceramics were not used for applications that required a combination of strength and toughness because of the inherent brittleness of ceramic materials. In those applications (e.g. high temperature cyclical loading) high strength is important, but what really matters is toughness. Ceramics shatter, metals yield. The key to making use of all of the good high temperature properties of ceramics (especially the low cost of the natural materials used to make them) is to somehow toughen them so that they behave more like metals yet still retain the properties that make ceramics desirable.[1]

Currently, only metals and metal matrix composites are used for high temperature (around 1000°C) gas turbine applications in the aerospace industry due to their high strength and stiffness. However, these materials cannot go higher than 1100°C and are costly and of high density.[2] The next phase of high temperature materials needs to be designed for use up to 1400-1500°C.

A ceramic based material would seem to be the likely answer for this next phase of materials because many ceramics are stable above 1500°C. Since ceramics are inherently brittle, a second, more ductile, phase is required to give the material the required toughness and the capability to withstand the cyclic, high temperature, long life use required. In

addition the composite must have good oxidation characteristics due to its potential use in air.

When designing a new material there are three basic items to look at: properties required, fabrication processes, and selection mechanisms. The required properties have already been stated; however, in other material design problems one would not only look at mechanical and thermal properties required but also optical and electronic properties required for use. Fabrication processes are important because this is where the benefits of using a ceramic could be outweighed by fabrication time and costs. Likewise it is useless to make a material that meets the desired properties but cannot be formed or machined into the desired shapes. Selection mechanisms are necessary to determine out of what to make the final material. Important questions to answer when determining what to use to make a new material are:

a. melting temperature

b. density

c. decomposition temperature

d. strength

e. fracture resistance

f. thermal expansion/conductivity

g. electronic/optical properties

h. phase compatibility

i. dimensional compatibility/stability.[3]

The first decision was to not use metals primarily because of their low melting temperatures and high densities. Next the matrix and the reinforcement phases should necessarily be oxides as they need to have good oxidation resistance (borides and high temperature carbides (with the exception of SiC) rapidly oxidize). So to have materials that

exhibit good high temperature properties, are not adversely affected by an oxygen environment, and are available, one comes up with a short list of alumina, mullite, SiC, and $MoSi_2$. Since alumina and mullite are stable, high temperature oxides and are potentially good barriers against oxygen diffusion, they would be viable candidates for matrix materials. SiC and $MoSi_2$, although oxidizable, both form protective layers of amorphous silica which limit the rate of oxidation to temperatures up to 1600° C and thus are good candidates for high temperature reinforcement.[4] Additionally, mullite and alumina cannot be used as a matrix and reinforcement together because of the difference in coefficients of thermal expansion.

Now to see how the choice of phases work together (answering some of the above questions). Alumina and either SiC or $MoSi_2$ are not phase compatible due to the tendency to combine and form mullite at high temperatures.[4] So the possibilities are confined to a mullite matrix with either SiC or $MoSi_2$ as the reinforcing phase.

A proposed dispersed phase is $MoSi_2$ which has long been used for heating elements in furnaces due to its capability of forming a protective amorphous SiO_2 coating when exposed to oxygen at high temperatures. In addition, $MoSi_2$ undergoes a brittle to ductile transition at about 1000°C giving it the ability to act as the ductile phase in the composite. So far, no one has investigated the use of a mullite matrix - $MoSi_2$ reinforced composite for high temperature use (other than oxidation studies).

GOAL OF THE RESEARCH

The main objective is to fabricate a material for use in aerospace applications at temperatures ranging from ambient to 1400° - 1500°C. This study will accomplish the preliminary steps to attain this objective using an $MoSi_2$ reinforced - mullite matrix as follows:

a. Determine the phase stability of $MoSi_2$ in mullite (initial characterization by x-ray diffraction and scanning electron microscope).

b. Process the mullite matrix - $MoSi_2$ reinforced composite by both hot pressing for mechanical testing and by pressureless sintering to achieve useful final densities.

c. Determine if the reinforcement phase has a toughening and strengthening effect as compared to the monolithic mullite matrix at low temperatures.

d. Determine oxidation behavior of the composite at high temperatures (will it strengthen, weaken, toughen, etc. after exposure to high temperatures). If this research shows improvement of the mechanical properties of the composite as opposed to the monolithic matrix at low temperatures, then high temperature testing -- strength, toughness, creep resistance, etc. and characterization studies will be performed to meet the overall main objective as stated above.

CHAPTER 2
BACKGROUND

2.1 COLLOIDAL SYSTEMS

A colloidal suspension is one in which the particles in suspension are much larger in size than the molecules of the solvent,[5] and around one nanometer to one micrometer. There is, however, no sharp distinction between colloidal and non-colloidal systems.[6] There are three types of colloidal systems:

(1) Colloidal dispersions which are two phased systems. This system is thermodynamically unstable.[5]

(2) True solutions of macromolecular material. This system is thermodynamically stable

(3) Association colloids -- colloidal electrolytes.[6]

The distinguishing feature of all colloidal systems is that the area of contact between the dispersed particles and the dispersion medium is relatively large[4] (large surface areas of particles).

2.1.1 LONDON-VAN DER WAALS INTERACTIONS

Of the many forces used to describe the interaction of matter, London-van der Waals interactions are of the most consequence in ceramic processing. These interactions are important because, when working with small particles, the forces are strong and long range enough to cause agglomeration of like particles. This force is operative over short distances (one nanometer) and decreases with the sixth power of the separation distance between particles, but is additive which gives the affect of long range attractions.[6]

Hamaker developed the following expression for the London-van der Waals particle - particle interaction energy, V_A, between particles separated by the short distance H:[7]

$$V_A = \frac{-A}{12}\left[\frac{y}{x^2+xy+x} + \frac{1}{x^2+xy+x+y} + 2\ln\left(\frac{x^2+xy+x}{x^2+xy+x+y}\right)\right] \qquad \text{Equation 2.1}$$

where $x = \frac{H}{a_1 + a_2}$, $y = \frac{a_1}{a_2}$

If the particles are taken to be perfect spheres ($a_1 = a_2 = a$) then Equation 2.1 becomes:

$$V_A = \frac{-A}{12}\left[\frac{1}{x(x+2)} + \frac{1}{(x+1)^2} + 2\ln\left(\frac{x(x+2)}{(x+1)^2}\right)\right] \qquad \text{Equation 2.2}$$

And if H is taken to be much less than a ($H \ll a$) Equation 2.2 simplifies to:

$$V_A = \frac{-Aa}{12H} \qquad \text{Equation 2.3}$$

A in the above equations is a constant -- referred to as the Hamaker constant . In vacuum:[8]

$$A = \pi^2 q^2 \alpha^2 I \qquad \text{Equation 2.4}$$

q = atomic density of the particle

α = polarizability

I = ionization potential.

When a liquid is used as the dispersion medium (as opposed to a vacuum), the van der Waals interaction energy is lowered and the constant A in the previous equation must be replaced by an effective Hamaker constant. Consider two particles (1, 2) in a dispersion medium (3). In order to bring the two particles together, liquid must be displaced resulting in particle-particle (A_{12}) and particle medium interactions (A_{13}, A_{23}). (See Figure 2.1) Combining these gives the effective Hamaker constant A_{132}:

$$A_{132} = A_{12} + A_{33} - A_{13} - A_{23} \qquad \text{Equation 2.5}$$

If the attraction between unlike phases is taken to be the geometric mean then Equation 2.5 becomes:

$$A_{132} = \left(\sqrt{A_{11}} - \sqrt{A_{33}}\right)\left(\sqrt{A_{22}} - \sqrt{A_{33}}\right) \qquad \text{Equation 2.6}$$

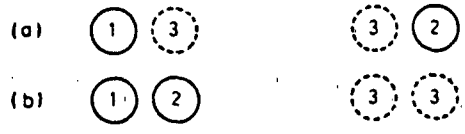

Figure 2.1 Particle-particle and particle-dispersion medium interactions. (a) particles 1 and 2 far apart in dispersion medium 3, (b) particles 1 and 2 close together displacing dispersion medium.[5]

If the two particles are of the same material, then Equation 2.6 becomes:[6]

$$A_{131} = (\sqrt{A_{11}} - \sqrt{A_{33}})^2 \qquad \text{Equation 2.7}$$

2.1.2 DOUBLE LAYER AND DLVO FORCES

As discussed previously, particle - particle attractions are governed by London-van der Waals attractions. However, if those particles are placed in a polar medium (H_2O), then those particles can acquire an electrical surface charge via ionization, ion adsorption, and/or ion dissolution. This surface charge acquisition sets up another type of interparticle interaction. Counter ions are attracted towards the surface, and co-ions are repelled away from the surface. This leads to a double layer consisting of an inner region (adsorbed ions) and a diffuse region where ions are distributed via the influence of electrical forces and random thermal motion.

Stern (1924) proposed a model in which the double layer is described. The two layers are separated by a plane (Stern Plane) located at approximately one hydrated ion radius from the particle surface. Adsorbed ions that are attached strongly enough to the particle surface not to be loosened by thermal agitation make up the inner or Stern layer. In the Stern layer the electric potential goes from ψ_0 at the particle surface to ψ_D at the Stern Plane and then decays to zero in the diffuse outer layer. Those ions that remain close to but are not specifically adsorbed are the diffuse double layer. The diffuse outer layer ends when the ion concentration is that of the dispersion medium. The Debye-Huckel length is used to give the thickness of the double layer and is of the order $3/\kappa$ to $4/\kappa$. κ is given by (for spherical particles):[5]

$$\kappa = \left(\frac{4\pi e^2 \Sigma(c_i z_i^2)}{\varepsilon k T}\right)^{\frac{1}{2}} \qquad \text{Equation 2.8}$$

e = charge on an electron

k = Boltzmann's constant

T = absolute temperature

ε = dielectric constant of the dispersion medium

c_i = concentration of the ionic species i

z_i = the valence of the ionic species i.

The Stern potential ψ_D, while easily defined is difficult to measure. It can be estimated, however, from electrokinetic measurements. Electrokinetic measurements are made based on the potential at the surface of shear between the charged surface and the solution. This potential is called the electrokinetic or ζ potential.

The double layer theory is important because it gives a picture of what is happening between dispersed particles and between the particles and the dispersion medium. From this double layer theory, Deryagin, Landau, Verwey, and Overbeek (DLVO)[6] developed a quantitative theory which involves estimation of the repulsive overlap of the electric double layer, and the attractive London - van der Waals energy. The electric double layer repulsive (usually) forces (V_R) can be provided in two distinct situations: (1) if the surface charge is the result of the adsorption of ions, then the surface potential remains constant and the surface charge density adjusts accordingly, and (2) if the surface charge is the result of ionization, then the surface charge density remains constant and the surface potential adjusts accordingly. These two cases are given below (for equal spheres):[6]

$$V_R = 2\pi\varepsilon a \Psi_D^2 \ln(1+\exp[-\kappa H]) \qquad \text{Equation 2.9}$$

$$V_R = 2\pi\varepsilon a \Psi_D^2 \ln(1-\exp[-\kappa H]) \qquad \text{Equation 2.10}$$

ε = permittivity of the dispersion medium

a = particle radius

ψ_D = Stern layer potential

κ = Debye-Huckel length

H = particle-particle separation

Having defined the attractive and repulsive energies (V_A, V_R) (albeit by simple spherical models -- the concepts are the same). The total energy is given by:

$$V_T = V_A + V_R \qquad \text{Equation 2.11}$$

This is the relation that was accomplished by the DLVO theory. So for particle-particle interactions, the London - van der Waals energy does not change (in a given system) but the double layer repulsive forces can be changed (see Figure 2.2).[6]

2.1.3 COLLOIDAL SUSPENSIONS

One of the keys to successful ceramic processing is to begin with a highly dense green compact with a uniform pore distribution since a highly dense green compact will generally have a higher sintered density. The key in achieving a highly dense green body is particle packing rather than agglomerate packing. Since van der Waals forces tend to cause particles in suspensions to form agglomerates, the DLVO repulsive energy theory may be used to counteract the tendency towards agglomeration with the ideal case being one in which each particle is "protected" by its double layer, i.e. repulsive energy high enough to counteract the attractive energy.[8,9] (See Figure 2.3)

Manipulating the double layer electrostatic energy may be accomplished by manipulating the zeta potential (surface charge). Increasing the zeta potential affects the total interaction energy as shown in Figure 2.4.[10] The most common method to manipulate the zeta potential is by changing the pH of the system. Figures 2.5 and 2.6 show the affect that varying the pH can have on the zeta potential. Increasing the zeta potential decreases the binding energy thus increasing the magnitude of repulsion between particles. So systems with highly repulsive forces (high zeta potentials) tend to pack as single particles rather than as agglomerates resulting in denser green bodies (see Figure 2.7).[11-14]

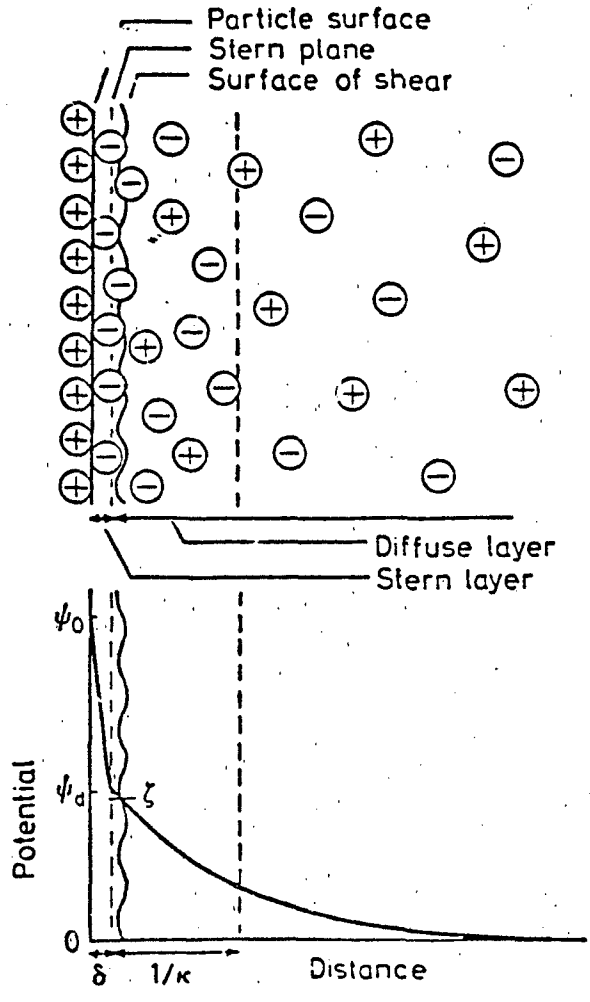

Figure 2.2 Schematic representation of the structure of the electric double layer according to Stern's theory.[5]

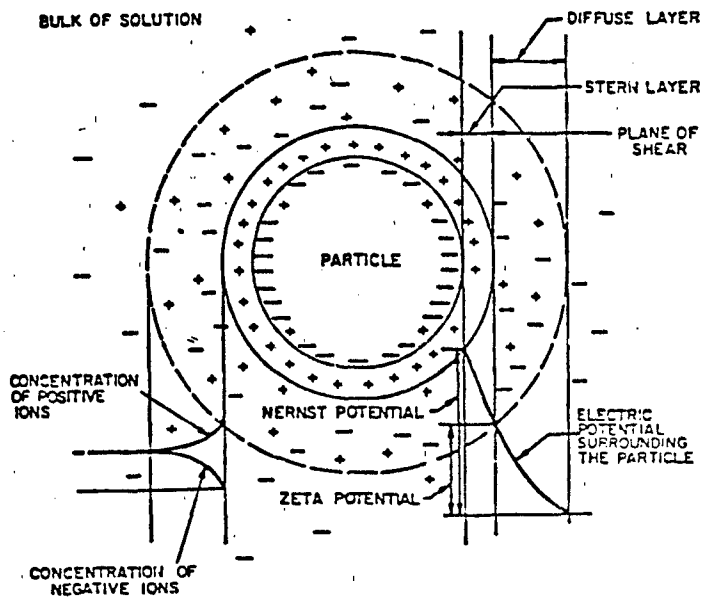

Figure 2.3 Schematic representation of the electric double layer around a particle.[8]

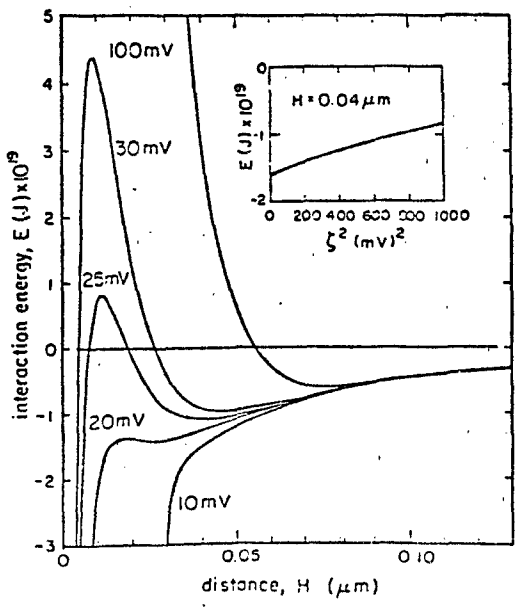

Figure 2.4 The influence of zeta potential on the total interaction energy for a 1.0 μm particle; $\kappa = 10^6\,cm^{-1}$; $A = 10^{-19}\,J$.[9]

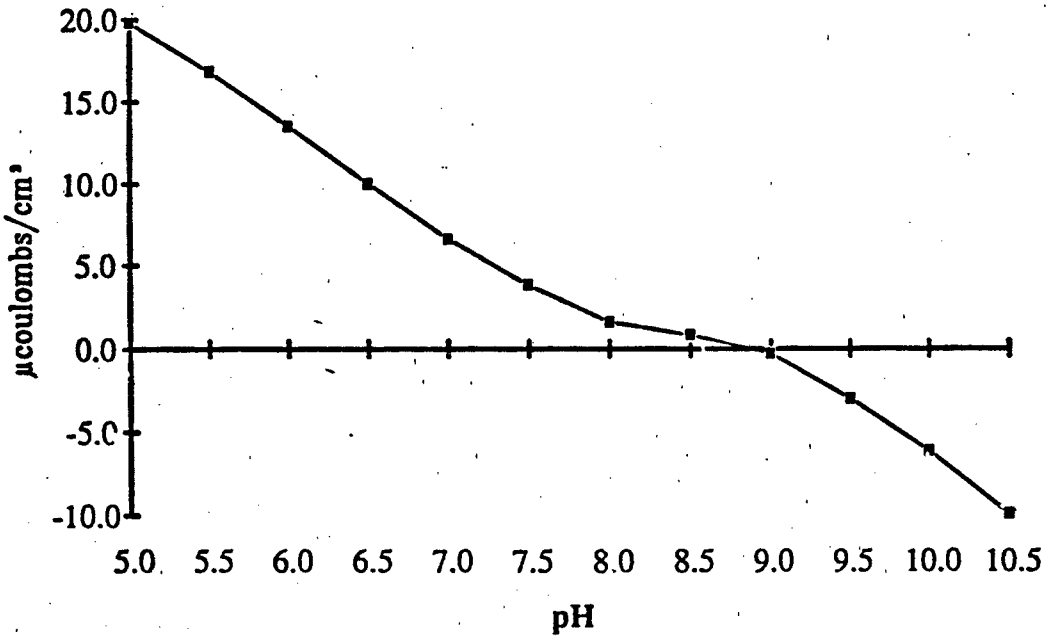

Figure 2.5 Surface charge of AKP-30 (α-alumina).[12]

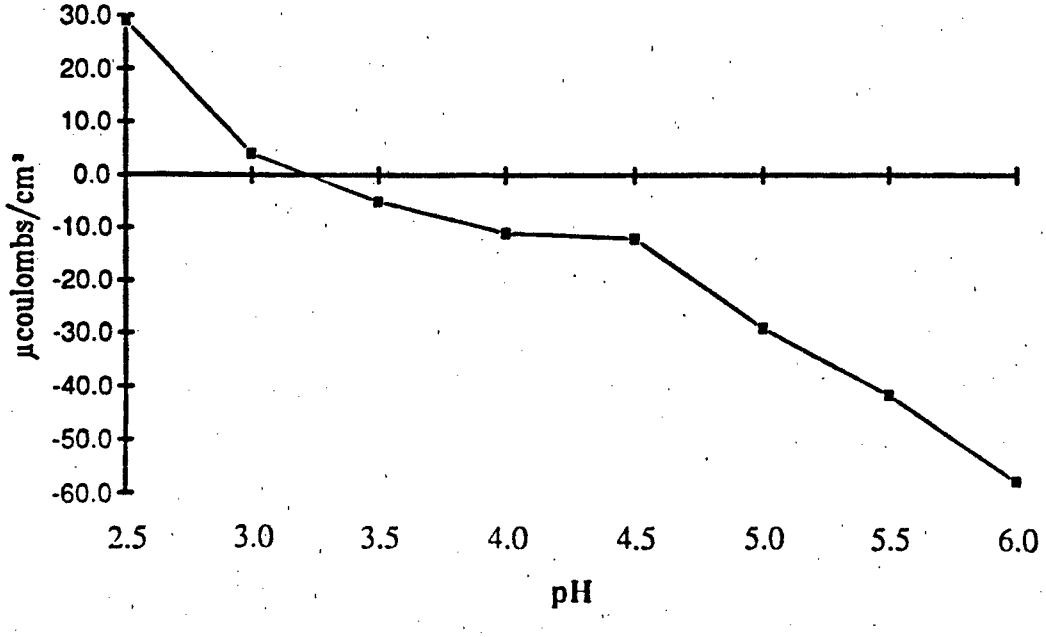

Figure 2.6 Surface charge of amorphous silica particles.[10]

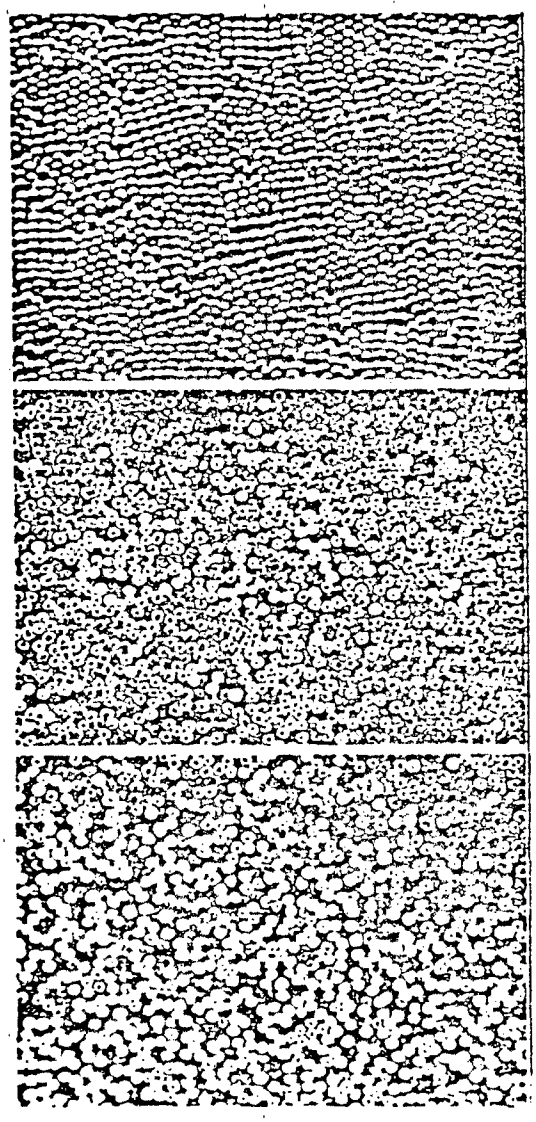

Figure 2.7 Microstructures of particle domain formed by centrifugal consolidation of SiO_2 colloidal suspensions at top $\zeta = 110$ mV, middle $\zeta = 68$ mV, and botton $\zeta = 0$ mV; average particle diameter is 0.7 μm.[8]

2.1.4 ALUMINA AND SILICA

Alumina and silica are commonly used ceramics because of their availability, properties, and propensity to form mullite when combined. In order to successfully use them in processing, one needs to know their surface characteristics -- zeta potential/surface charge. Figures 2.5 and 2.6 show the surface charge of alumina and silica.

Alumina forms a hydroxyl group on its surface, and depending on the pH, can react with an H_3O^+ ion to form a positive site or react with an OH^- ion to form a negative site depending on which side of the neutral range the pH is (around 8.5). This means that alumina can be processed in either acidic or basic conditions, depending upon the surface characteristics desired.

Silica, because of its structure, acts much differently. The building blocks which make up silica are SiO_4 tetrahedra, which share corners resulting in an overall composition of SiO_2. Each tetrahedron has a -4 charge overall so the tetrahedra located at the surface of the particle which don't share all 4 corners will be strongly negative. As a result, SiO_2 is negative across most of the pH spectrum.[13,14]

2.1.5 HETEROCOAGULATION

Heterocoagulation is the coagulation of dissimilar particles.[5] It can occur when the attractive forces (V_A) dominate over the repulsive forces (V_R), or:

$$|V_A| > |V_R| \qquad \text{Equation 2.12}$$

For this to occur, in the general case, the Hamaker constant (A) is positive and the zeta potentials (or surface charges) on the particles are of opposite signs.[8] So to ensure the occurrence of heterocoagulation, the particles in the suspension should (generally) be oppositely charged. Healy, et al.[15] modeled how this occurs with two oxides having

displaced zeta potential curves as shown in Figure 2.8. Between the isoelectric points (iep) of the two oxides, one oxide will be positively charged and one negatively charged and thus the two will attract. The curve below shows the predicted coagulation behavior both between the same oxide and between the two different oxides. A value of W equal to 0 means a flocculated (or coagulated system). This model predicts the coagulating behavior between the two iep's of the two oxides. Healy backed up his model with experimentation in the Al_2O_3-SnO_2 system as shown in Figure 2.9. However the flocculated state doesn't correspond directly to his model which would predict flocculation between pH 4.5 and 9. In effect, the mixed system at equilibrium produces a new colloidal system with both particles having iep values in the range of pH 7-8. This effect may be explained by the magnitude of charges on the particles. Close to the iep of one particle system, those particles will have a weak surface charge where the other particles will have a strong charge. The different particles will still attract, but the particles with the high magnitude of charge will be repulsed by like particles with those repulsive charges overcoming the weaker attractive charges. The fact that interparticle behavior can be influenced by changing the surface charge (by changing pH) is useful in ceramic processing. Coating large particles with small particles, yet keeping the overall system dispersed is one of the key uses for heterocoagulation.

2.1.6 PRESSURE FILTRATION[16]

Pressure filtration is widely used to concentrate the solids in slurries and can be used to consolidate complex shapes. Particles form a consolidated layer on the filter as the fluid is forced through the system. Once this consolidated layer is formed, its permeability and thickness control the filtration kinetics.[16] Filtration kinetics obey Darcy's Law:[17]

$$J = \frac{kP}{\mu x}$$

Equation 2.13

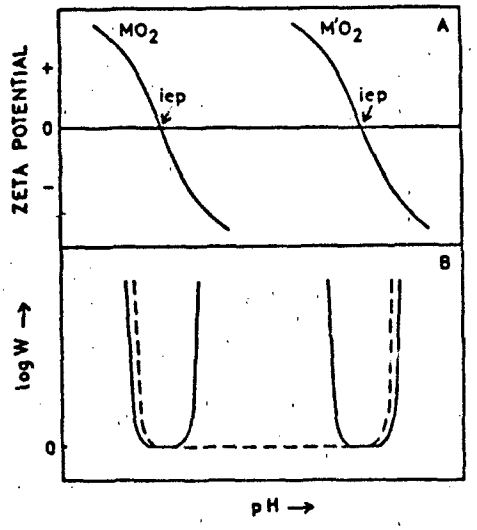

Figure 2.8 Schematic representation of the variation of (a) ζ potential of two oxides as a function of pH and (b) the predicted coagulation behavior expressed as a stability ratio for these separate oxides (solid) and mixed system of two oxides (dashed).[14]

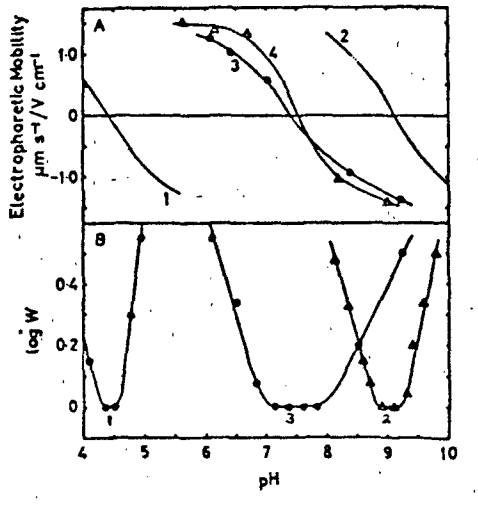

Figure 2.9 Electrophoretic mobility and coagulation behavior in the system SnO_2-Al_2O_3. (a) Mobility as a function of pH for (1) SnO_2, (2) Al_2O_3, (3) SnO_2 in Al_2O_3 supernatant, and (4) Al_2O_3 in SnO_2 supernatant. (b) Log stability ratios for (1) SnO_2, (2) Al_2O_3, and (3) mixed SnO_2-Al_2O_3.[14]

J = flux (fluid volume per unit area per unit time)

x = consolidated layer thickness

P = pressure difference across the consolidated layer

k = permeability of the layers

μ = viscosity of the fluid

The permeability of the consolidated layer depends on the number and size of channels through the consolidated layer which in turn depends upon the particle size and particle arrangement.

Particle arrangement is influenced by applied pressure with packing density increasing (generally) with increasing applied pressure which results in decreasing permeability (generally) with increasing applied pressure. Particle arrangement is also influenced by the interparticle forces in the system. Those systems with strongly attractive interparticle forces are more difficult to arrange during consolidation than strongly repulsive particles which readily pack to their optimum density.[18]

Assuming that the volume displaced by the moving plunger is equal to the volume of fluid forced through the filter, Darcy's Law can be integrated to obtain:[16]

$$d = \left[2\frac{k}{\mu}\left(\frac{v_l}{v_o} - 1\right)Pt\right]^{\frac{1}{2}}$$

Equation 2.14

d = plunger displacement

t = filtration time

P = applied pressure

k = permeability of the solid layer

μ = viscosity of the fluid

v_l = volume fraction of solids in the consolidated layer

v_o = volume fraction of solids in the slurry

This shows that pressure filtration should exhibit parabolic rate kinetics. Another interesting application of Equation 2.14 is that it can be rearranged to give the time required to consolidate a body that will have a thickness x_s after it is fully densified during sintering:[16]

$$t = \left[\left(\frac{\mu}{2kP}\right)\left(\frac{v_l}{v_o} - 1\right)v_l^{\frac{2}{3}}\right]x_s^2 \qquad \text{Equation 2.15}$$

Applying standard values for an alumina system, Lange[16] found that the coefficients are 1 min/cm^2 for flocced and 0.4 min/cm^2 for dispersed slurries ($v_o = 0.15$ for the flocced state and 0.5 for the dispersed state) for a pressure of 70 MPa. Conventional slip casting periods would be on the order of 500 times greater.

2.2 TOUGHNESS.

Toughness is a material property which gives a measure of resistance to crack propagation when the material is subjected to mechanical or thermal stress.[19] One approach is to consider the energy demand curve for crack propagation in conjunction with the energy release curve. This approach, modeled by Griffith is applicable to ideal brittle systems, i.e. ceramic systems. Some modifications are required when dealing with non-ideal brittle systems, but since ceramic systems are the topic, the following discussion will focus on the unmodified model.

Griffith proposed that a brittle material contains a population of fine cracks which produce a stress concentration of sufficient magnitude so that the theoretical cohesive strength is reached in localized regions at a nominal stress which is well below the theoretical value. When one of the cracks spreads, it provides an increase in the fracture surface area. This requires an increase in surface energy which is supplied by the elastic strain energy that is released as the crack spreads. As Griffith states, "A crack will

propagate when the decrease in elastic strain energy is at least equal to the energy required to create the new crack surface."[20]

When a crack is formed there is a resulting decrease in strain energy. If an elliptical crack is formed in a plate, then the elastic strain energy per unit of plate thickness is equal to:

$$U_E = -\frac{\pi c^2 \sigma^2}{E} \qquad \text{Equation 2.16}$$

where σ is the tensile stress acting normal to the crack of length 2c. (It is negative because crack growth releases elastic strain energy.) The crack's surface energy is:

$$U_s = 4c\gamma_s \qquad \text{Equation 2.17}$$

and the resulting total change in potential energy from the creation of the crack is:

$$\Delta U = U_s + U_E \qquad \text{Equation 2.18}$$

According to Griffith's criterion, the crack will propagate under a constant applied stress if an incremental increase in crack length produces no change in the total energy of the system. That is, the increased surface energy is compensated by a decrease in elastic strain energy.

$$\frac{\partial U}{\partial c} = 0 \qquad \text{Equation 2.19}$$

$$4\gamma_s - \frac{2\pi c \sigma^2}{E} = 0 \qquad \text{Equation 2.20}$$

$$\sigma = \left(\frac{2E\gamma_s}{\pi c}\right)^{\frac{1}{2}} \qquad \text{Equation 2.21}$$

Thus, the stress required to propagate a crack is inversely proportional to the square root of the crack length.[20]

To develop a tough ceramic where stable cracks can form and not propagate, the energy demand curve (U_S) must change from non-linear to concave upwards so that the slope of the energy release curve does not catch up with the demand curve unless higher

levels of stress are applied. This is impossible for single phase, homogeneous brittle materials, but can be achieved with multi-phase brittle ceramics.

In a multi-phase ceramic, a crack in the less tough component will propagate but it may encounter the stronger component and then have two choices: either cut across this phase or detour around it. Either course means that the energy demand will increase as a step function, and crack propagation will stop, unless the applied stress is appropriately increased. A whole series of such encounters produces a series of steps in energy demand and, as a result, the energy demand curve changes from linear to curved. In order for the curve to be concave upwards the dispersed phase must be tougher than the matrix. If the dispersed phase is not tougher than the matrix, cracks may propagate through the material even easier than in the homogeneous matrix material.

This process is depicted in Figure 2.10 where, in a multi-phase ceramic, an initial crack of length c_0 will begin to grow under a stress σ_0 but it will be stopped at length c_1 when the slope of the energy demand curve at c_1 exceeds the slope of the energy release curve. Repeated application of this step mechanism and successively higher applied stresses by which the crack proceeds from instability (moving), to stability (static), eventually produces a situation where the energy release curve intersects the energy demand curve. At the point of intersection the crack will grow spontaneously and catastrophically. The value (γ_c) of the rate of energy absorption at the point of crack instability, i.e. at the point of intersection of the two curves, is important when considering the toughness of a multiphase ceramic. This value is the critical strain energy release rate, and has the value of the maximum slope attained by the energy demand curve.

γ_c can be regarded as a material constant whose value depends on a combination of factors:

a. the type of second phase (tougher or less tough than the matrix);

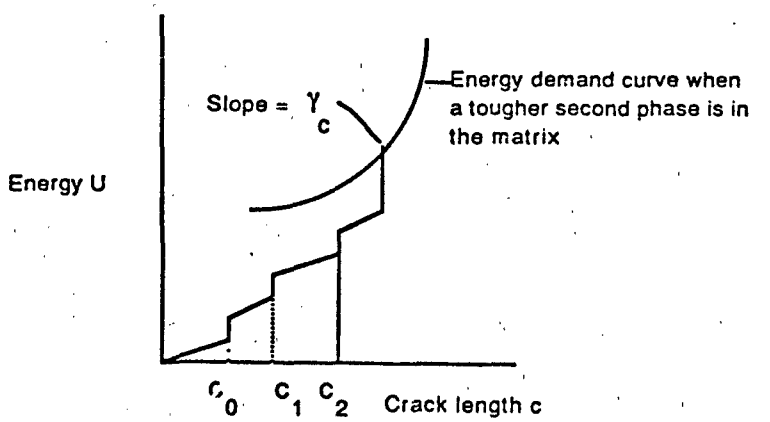

Figure 2.10 Energy demand and energy release curves in a multiphase ceramic.[21]

b. The size of second phase particles (small particles may become "invisible" to the crack, large ones may depend too much on the interfacial bonds); and

c. volume (increase here results in an increase in γ_c until it becomes large enough to produce microscopic defects).

Interphase bonding is also important. Strong bonding between phases allows the composite to gain in toughness without losing the high strength of the matrix. Weak interfacial bonding will increase the energy demand, i.e. toughness by the definition we are using, as the crack detours, but the crack is easier to initiate and ultimate strength is thereby reduced. As a result, the high strength ceramic matrix composites will provide attractive engineering materials if a second tougher phase is dispersed in the high strength matrix material. [21]

So something needs to be done to the ceramic matrix to assist it in stopping the catastrophic propagation of cracks. Several authors have discussed different toughening mechanisms, but they all pretty much boil down to:

a. load transfer

b. crack deflection

c. crack impediment

d. crack bridging

e. microcracking

f. phase transformation.[22]

2.2.1 LOAD TRANSFER

This first mechanism, load transfer from a low strength, high toughness matrix to high strength, usually brittle fibers due to Young's modulus of the fiber (E_f) being greater than that of the matrix (E_m), is the fundamental concept of most polymeric and metal matrix

composites. The extent of toughening due to load transfer with fibers generally increases as the E_f/E_m ratio and the volume fraction (V_f) of fibers increase. Significant mechanical property improvements have been achieved with low densities of fibers in bodies of low Young's modulus such as gypsum, plaster, cement, and refractories. Progress has also been made by introducing Al_2O_3, graphite or SiC fibers in silicate based glass or crystallized glass matrices where E_f/E_m is only on the order of 3-6.

However, applying the load transfer mechanism to the more refractory ceramics (use above 1100° C for prolonged or cyclical use) is much more difficult. Most materials that can be used as fibers at these high temperatures have Young's moduli which are roughly equivalent to that of the ceramic matrix. Even those fibers that do have a higher modulus at room temperature rapidly lose that advantage as temperature increases.[19,23]

2.2.2 CRACK DEFLECTION

The second mechanism is analogous to prestressing concrete. The difference in this case is that the prestressing is accomplished by differences in thermal expansion between the fibers and the matrix. The general case is when cooling from processing temperatures, the fiber is in tension and the matrix is in compression. Even though the compressive stresses in the matrix decrease with the cube of the distance from the fiber surface, useful levels of compressive stress can be achieved using a high density of fibers. This mechanism, although real, is still not totally understood. For example: how much will the compressive stress in the matrix hold up the crack's progress before the combination of the tensile stress in the fibers and the applied stress concentration ahead of the crack breaks the fiber thus relaxing the compressive stress of the matrix?[19,23]

In particulate reinforced ceramics, research has shown that an advancing crack was attracted to the tensile region surrounding a particulate. Countering this advance is the

compressive stress in the matrix. Results of the addition of TiB_2 particulates to a SiC matrix showed almost an 80% increase over the monolithic matrix of the crack growth resistance.[24]

2.2.3 CRACK IMPEDIMENT

The third mechanism is the use of crack impeding second phases. The extreme case is to completely arrest cracks. This would generally require metal wires (having sufficient toughness and strength). However ductile wires generally can't withstand the amount of heat required in either processing or use. Since high temperature, oxidation resistant fibers are also generally brittle, they too would lack the toughness to resist fracture.

Since crack arrest is not feasible, the next best method is to insert particles which are more difficult to fracture than the matrix. Then the crack is temporarily impeded by the tougher particles. The crack will then bow out between particles and either stop growth or continue until it reaches a critical breaking condition as proposed in Lange's line tension model (see Figure 2.11). When using fibers, one achieves the maximum benefit with uniaxial fibers aligned with the principal stress. That benefit goes to zero as the fiber stress angle increases to 90°. Further, the toughness is not significant unless the fiber spacing is less than the flaw size thus requiring a high density of fibers. In contrast to the highly directional effects of line tension toughening with unidirectional fibers, particles would give perfect, or nearly perfect, isotropy of toughening. However, the level of toughening would be substantially less since cracks can frequently go around some of the particles. Additionally, if the particles are too small in relation to the crack, the crack will move right through the particle as if it wasn't there. If the particles are extraordinarily large, the line tension toughening effect is lost as the interfacial region plays the important interaction role.

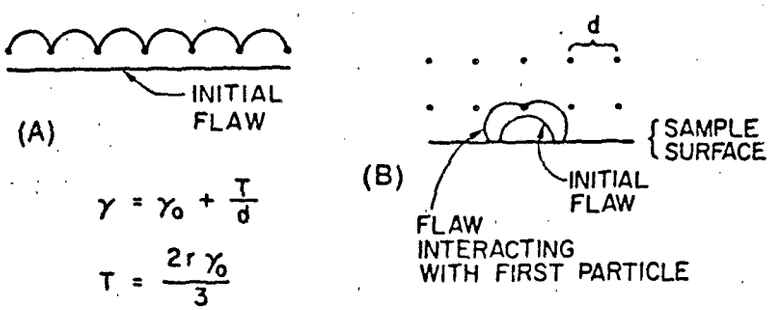

Figure 2.11 Simplified line tension toughening model. (a) Interaction between large, plane crack with series of uniformly spaced particles; (b) Interaction of small crack with particle array. Equations are valid for either situation. Note significant reduction in fracture energy increase when flaw size approaches spacing between particles. d = particle spacing, γ_o = matrix fracture energy, r = flaw radius.[23]

Control of stresses from particle-matrix property mismatches are important in predicting the degree of crack-particle interactions since cracks prefer to propagate normal to tensile stresses and parallel with compressive stresses. Cracks are deflected around spherical particles in hydrostatic tension but attracted directly into particles under hydrostatic compression (see Figure 2.12). Therefore, maximum crack-particle interaction occurs when the crack approaches the particle close enough for these stresses to become effective. Close approach is required because of the rapid ($1/r^3$) decrease in stress away from the particle-matrix interface. Thus, the way to make this mechanism effective is to have a high density of particles with mismatch stresses with the matrix. Similar consideration shows that particles, whether spherical or elongated, with one pronounced axis of compression should have similar crack "attracting" effects. The main sources of effective mismatch stress are thermal expansion or phase transformation, but some contribution can occur due to elastic differences.[23]

2.2.4 CRACK BRIDGING

Substantial toughening effects (an increase in fracture toughness of a factor of at least three to five)[23] can be attained through the proper use of discontinous, elastic second phases. The resultant toughening is caused by bridging of the crack surfaces by the strong reinforcing phase which applies a closure force on the crack. This is also usually supplemented by a contribution of pullout of the reinforcement.

How does this mechanism work? When the reinforcement is partially debonded it bridges the crack surfaces thus pinning the crack surfaces together and increasing the resistance to crack extension. Based on the energy dissipation/energy balance approach, the crack -bridging contribution to the toughness is:

$$K_{IC}^c = \sqrt{\left[E^c\left(J^m+\Delta J^{cb}\right)\right]} = \sqrt{(E^c J^c)} \qquad \text{Equation 2.22}$$

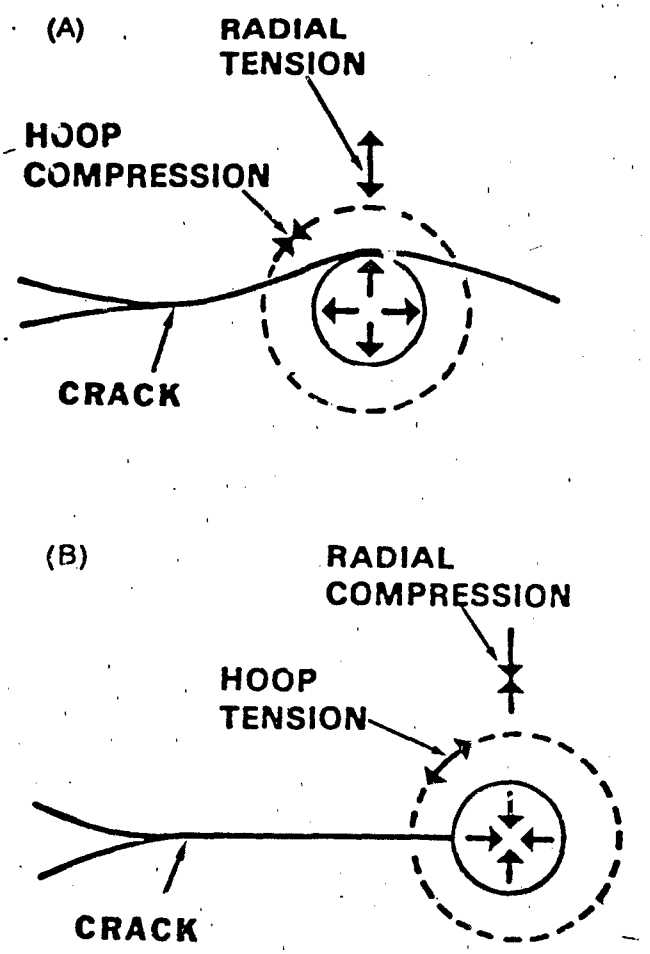

Figure 2.12 Crack particle interactions. (a) Schematic of interaction of crack with particle in hydrostatic tension ($\alpha_p > \alpha_m$); (b) with particle in hydrostatic compression ($\alpha_p < \alpha_m$). Since cracks propagate parallel with compressive stresses and perpendicular to tensile stresses, in case (a) the crack will tend to be deflected around the particle, where in case (b), the crack will be attracted directly into the particle. There is a high probability that the crack reaching particle in (b) does not fully relieve the compressive stress in the particle so this interaction significantly inhibits the motion of the crack making it a more effective toughening mechanism than case (a).[23]

$$K^m = \sqrt{(E^m J^m)} \qquad \text{Equation 2.23}$$

where K_{IC} is the toughness (m is for matrix, c is for composite) and E is Young's modulus. ΔJ_{cb} and J_m are used to define the energy change associated with the bridging process and with crack extension in the matrix, respectively. These quantities are determined using the J-integral approach using the bridging stress/traction and the crack opening displacement. This mechanism is also related to the preceding and following mechanisms since crack impediment, microcracking, or both can be important factors in crack bridging.[25]

The requirements for pullout to occur are either a high transverse fracture toughness in the fibers or particles or poor bonding between the fiber or particles and the matrix. However too poor of a bond between the particles or fibers and the matrix (i.e. low τ) would be expected to make the composite weak and hence make potential gains in toughness of limited value.[23]

2.2.5 MICROCRACKING

The fifth mechanism, microcracking, is due to property mismatches which cause large localized stresses. Mismatches due to differences in thermal expansion and to phase transformation are the most common sources of significant mismatches. It seems the key is to manufacture materials in which the the particle size is below that required for spontaneous microcracking, but in the range where microcracks could be stress induced. The microcracks form a zone around large cracks, and the creation of that zone around the propagating crack would reduce the stresses near the crack tip giving rise to shielding. An alternate explanation is that the microcracked zone significantly increases the amount of fracture surface thus stopping the propagation of the crack. The toughness is expected to increase with increased particle size up to the particle size required for spontaneous

cracking. When microcracks are a result of coefficient of thermal expansion mismatches, one would expect that with increasing temperature toughness would diminish as the thermal stresses cause relaxation. Microcracks formed by transformation toughening would be temperature insensitive (unless the transformation reverses), but there would be a need to keep a cap on the volume of microcracks as interaction effec , may increase the likelihood of spontaneous transformation which could then cause the microcracks to link and become propagating macrocracks.[23,26,27]

The generation of small cracks only at, or near, the tip of a stressed crack by interaction of the crack-tip stress field with property mismatches between the matrix and the dispersed phase is of interest. The microcracks are generated due to the superposition of the high tensile stresses concentrated near the crack tip and the intrinsic mismatch stresses. The result is a microcracked "process" zone around the crack tip (see Figure 2.13). The design of systems in which microcracking would occur only in the high stress region of a highly stressed crack may be an important mechanism whereby the amount of strength limitation that microcracking may impose can be kept small, allowing this to be a mechanism of toughening while maintaining good properties.

An upper bound of fracture energy increases can be estimated, based on energy absorption by microcracking, by considering a cylindrical process zone of elliptical cross section around a through-the-specimen thickness, i.e. slit, crack (see Figure 2.13). Assume N platelet particles (lateral dimensions, l, and thickness, t) which will microcrack per unit width of the crack (i.e. unit dimensions in the plane of the crack, but perpendicular to its propagation) within a zone of major and minor axes L and αL ($\alpha<1$). Then the volume fraction of particles with cracks (along their two larger surfaces, i.e. total area $2L^2$ of the process zone is:

$$V_f = \frac{Nl^2t}{\pi\alpha L^2}$$

Equation 2.24

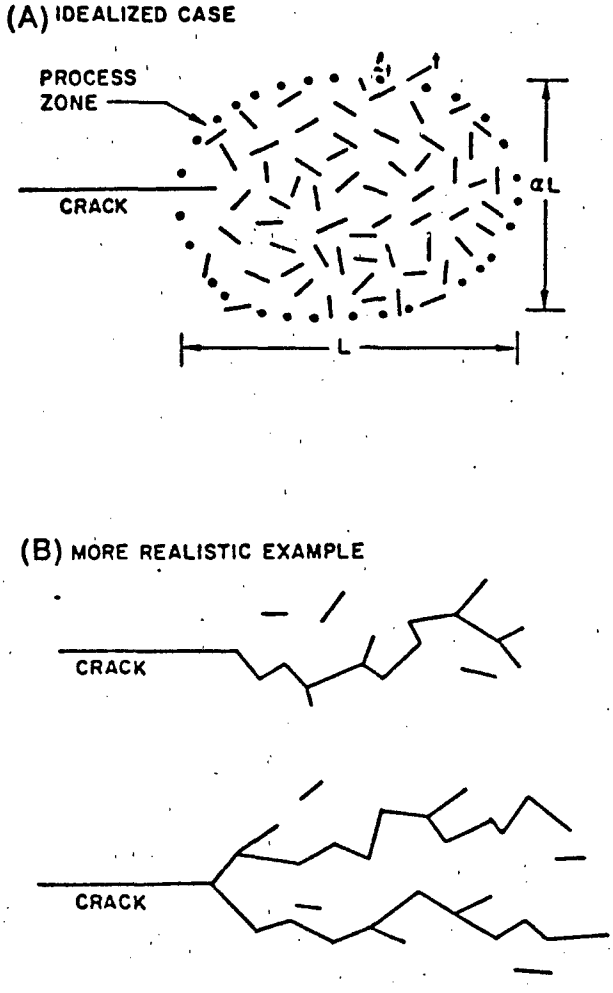

Figure 2.13 Microcracking (a) Idealized case of microcrack process zone around tip of crack; (b) more realistic examples of microcracking -- main crack propagates due to significant linkage with some microcracks generated.[23]

The surface energy, Γ, absorbed in generating 2N microcracks (1 on each side of a platelet) is:

$$\Gamma = 4\gamma_B NL^2 \qquad \text{Equation 2.25}$$

Where γ_B = the interfacial fracture energy (the factor of four comes from two microcracks per particle and two surfaces per microcrack).

The increase in fracture energy, $\Delta\gamma$, due to microcracking per unit area of advance of the main crack, then is

$$\Delta\gamma = \frac{\Gamma}{2L} = \frac{2\pi\gamma_B V_f L}{t} \qquad \text{Equation 2.26}$$

Thus the increase in γ due to microcracking is directly proportional to the boundary fracture energy, the volume fraction of particles which develop cracks (and hence generally of the V_f of particles themselves), and the process zone size, and inversely proportional to the particle dimension (thickness for platelets, or diameter for rods or spheres).

The above equation is however, an overestimate since the crack does not remain stationary as it generates many microcracks. Improved models which address, at least in part, the crack-microcrack interaction are more complex but give trends basically consistent with those of the above equation. The type of microcracks (i.e. forming along the particle-matrix interface or outward into the matrix from this interface) can also be important, but again trends are similar to the above equation, though γ_B is replaced by a crack-size-dependent local fracture energy that can range from γ_B up to γ_{pc}.

Note that the above equation directly and indirectly emphasizes small particle sizes. Besides being inversely proportional to t (or the diameter of rods or spheres), the process zone size is likely to increase as the particle-matrix mismatch strain ($\Delta\varepsilon$) increases.[23]

2.2.6 PHASE TRANSFORMATION

Concept six, phase transformation toughening, is a relatively recent and spectacular entrant to the field of ceramic toughening mechanisms. The concept is based on the idea that a phase transformation can be stress induced in a material in such a way that it decreases the driving force that is acting to propagate the cracks that are present, or can form under stress, in the material.[23] The way it works is that fine particles of an unstable crystal structure are inhibited by the matrix from transforming to the stable structure except in the presence of the high stresses near a crack tip under high stress. Smaller particles are inhibited from transforming by the matrix, apparently following a particle size dependence similar to that for microcracking. Thus, to have transformation only in the stress field of a crack, small particles are necessary to avoid spontaneous transformation of all particles. Strain energy is thus "trapped" in the matrix of the transformed layer, hence absorbing significant energy otherwise available for crack propagation.[26] Modeling of this mechanism is under way; for example, Lange gives:

$$K_c = \left[K_0^2 + \frac{2V_f E_c R\,(|\Delta G| - \Delta U f)}{1 - \nu^2} \right]^{\frac{1}{2}} \qquad \text{Equation 2.27}$$

ν = Poisson's ratio

R = thickness of the transformed zone

ΔG = the change in chemical free energy in the transformation

ΔU = strain energy associated with transformation

f = the fraction of strain energy not relieved by the transformation.

Particles may transform near a free, e.g. machined surface, providing some degree of compressive stress on the surface. This can give useful levels of apparent toughening where one is concerned with failure from surface flaws that are generally produced during machining processes. Note that, in either case (untransformed particles in the matrix or transformed particles at the machined surface), the effect increases with the volume of

particles. It is important to note that the generation of microcracks around the precipitates is believed to enhance the occurrence of the transformation and reduce the strain energy storage in the matrix, hence limiting the effectiveness of this mechanism (and again limiting particle sizes).

Phase transformation toughening has been identified in ZrO_2 bodies. It is also expected to occur in HfO_2, ZrO_2's close chemical analog. Both of these materials prefer to transform from the more dense high temperature tetragonal structure to the less dense monoclinic form at lower temperature with a significant lattice expansion in the c direction.[23]

Although six toughening mechanisms were discussed, all are interrelated as can be seen by the descriptions. This is also why different authors sometimes refer to only a few of the toughening mechanisms or call them different names, although the explanations generally run the gamut of those provided. Of the six mechanisms, only load transfer is generally not applicable to improving the toughness of advanced high temperature ceramics.

2.3 SINTERING

2.3.1 SOLID STATE SINTERING

Sintering is generally regarded as the process that transforms a porous green compact into a strong, dense ceramic. This occurs during firing by the transfer of material from one part of the structure to another. As material is transferred, the pores change in shape and size generally becoming more spherical in shape and smaller in size (see Figure 2.14). The driving force for this densification during firing is a change in free energy caused by the decrease in surface area and the lowering of the free energy by the

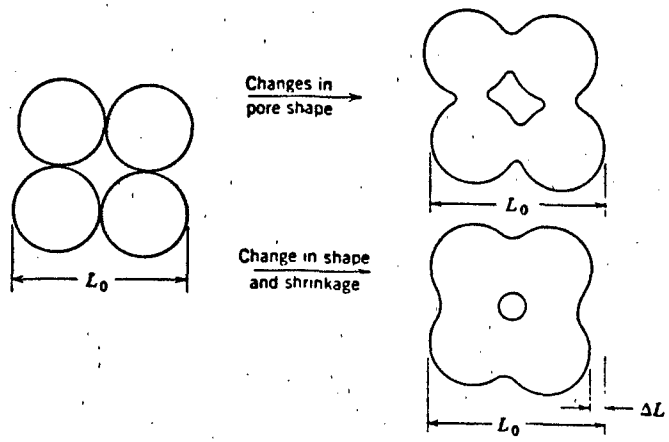

Figure 2.14 Changes in pore shape do not necessarily shrinkage[27]

elimination of solid vapor interfaces. As a result, solid - solid interfaces are formed but these are of a lower energy than the solid - vapor interfaces being replaced. Microscopically, the pressure difference and changes in the free energy across a curved surface are what affect the material transfer.

The curved surfaces being dealt with are the positive radius of curvature of the particle and the negative radius of the neck formed at the junction of the two particles. The difference in the free energy between these two areas provides a driving force for the transfer of material. Table 2.1 and Figure 2.15 describe and show the various paths for matter transport. It is interesting to note that only those transport paths that involve transfer of matter from the particle volume or from the grain boundary between particles causes shrinkage and pore elimination.

Solid state sintering is important because objects readily retain their shape -- the solid state is maintained at all times so that the object cannot slump or otherwise deform (other than through shrinkage) during the process. However, because it is solid state sintering, the high temperatures for prolonged periods of time that are generally required for densification could cause extended grain growth -- a situation that is undesirable for most structural ceramics.[28,29]

2.3.2 LIQUID PHASE SINTERING

Liquid phase sintering (or sintering in the presence of a reactive liquid) is another process that leads to densification. Generally this type of sintering is only used in certain systems and for certain applications because the essential part of this process is the solution and co-precipitation of solids to give increased grain size and density.

For liquid phase sintering to occur rapidly (so slumping or warpage does not occur), it is essential to have: (1) an appreciable amount of liquid phase, (2) an appreciable

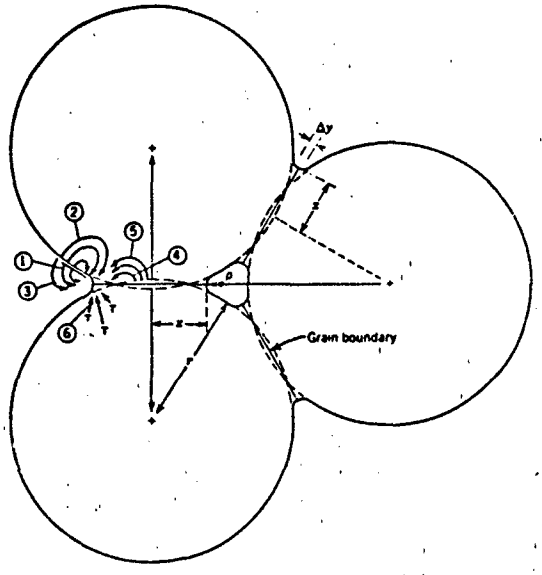

Figure 2.15 Alternative paths for matter transport during the initial stages of sintering[27]

Table 2.1 Alternate Paths for Matter Transport During the Initial Stages of Sintering.

Mechanism	Transport Path	Source of Matter	Sink of Matter
1	Surface Diffusion	Surface	Neck
2	Lattice Diffusion	Surface	Neck
3	Vapor Transport	Surface	Neck
4	Boundary Diffusion	Grain Boundary	Neck
5	Lattice Diffusion	Grain Boundary	Neck
6	Lattice Diffusion	Dislocations	Neck

solubility of the solid in the liquid, and (3) wetting of the solid by the liquid. In this case, the driving force for densification comes from the capillary pressure[27] (175-1750 psi in silicate systems depending upon particle size) of the liquid between the solid particles.

The advantages to this type of sintering are that densification is enhanced (liquid phase transport due to the high capillary forces at particle contact points) and the sintering temperatures are generally much lower than in solid state sintering. However, the liquid addition does remain in the body and since it has a lower melting temperature than the matrix, it can cause creep or other deleterious behavior at higher temperatures.[28,29]

2.3.3 VISCOUS PHASE SINTERING

Densification with the aid of a viscous liquid phase is the major firing process for the majority of silicate systems. A viscous liquid silicate is formed at or near the sintering temperature and acts as a bonding agent for the body. For this system to work, densification must occur without slumping or warping of the object being sintered (there can't be too much of the viscous phase and it can't be too viscous).

When two particles are in contact, there is a negative pressure at the neck which causes viscous flow of material into the pore region. The factors determining the vitrification rate are the pore size, viscosity of the overall composition, and the surface tension. During viscous phase sintering, coarsening and enlargement of pores do not occur. Rather pores are eliminated due to all of the pores having a pressure exerted on them equal to $2\gamma/r$ during the final stages of sintering.

The benefits to this type of sintering is the elimination of pores in the sintered body due to the rapid densification that occurs. However, disadvantages are in high temperature use as creep and other high temperature effects due to the presence of the viscous phase may become a problem.[28,29]

2.3.4 HOT PRESSING

The sintering mechanisms described thus far depend on capillary pressures to provide the driving force for densification. External pressure can also be applied, usually at the sintering temperature, which will increase the driving pressure for densification by acting against the internal pore pressure (see Figure 2.16). Advantages to hot pressing are that: the need for very fine particles is eliminated, large pores from non-uniform mixing are removed, and that a ceramic may be produced with a comparable density but a finer grain size or comparable grain size but higher density. The disadvantages of hot pressing oxide bodies are the expense and short life of dies used at high temperatures and the difficulties in making the process automatic to achieve high-speed production.

Densification during hot pressing can occur via all of the mechanisms discussed for the three sintering processes. In addition, due to the applied pressure, plastic deformation of particles which may occur due to the high stresses at particle contact points can also aid in the densification.[28,29]

2.4 MULLITE

Mullite is one of the most common phases found in industrial ceramics and is formed by the reaction:[30]

$$3Al_2O_3 + 2\,SiO_2 \rightarrow 3Al_2O_3 \cdot 2\,SiO_2$$

It is a stable phase from room temperature to 1828°C, has excellent creep resistance[31-33] (pure mullite ranges from around 5×10^{-8} - 3×10^{-6} s^{-1} at a constant 100 MPa stress from 1230° - 1430°C) and low thermal expansion[28] (3-5 x 10^{-6}/°C) thus lending it to high temperature use.[28,32,34] Mullite's mechanical properties are highly dependent on the processing conditions used to fabricate it with strength maintained from room temperature to 1500°C.[32,34-37] High temperature strength is highly dependent on the presence or

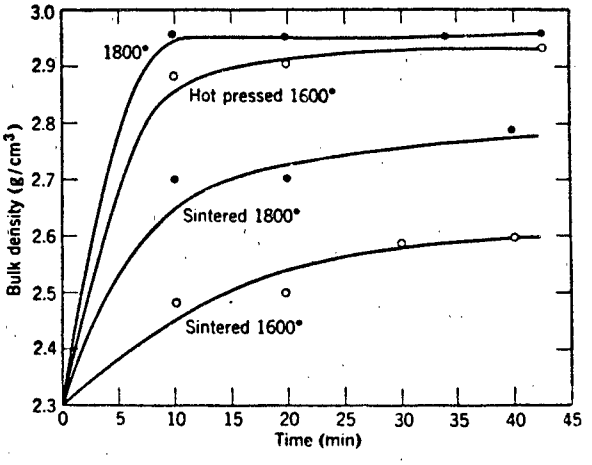

Figure 2.16 Densification of beryllia by sintering and by hot pressing at 2000 psi.[27]

elimination of glassy boundaries.[38,39] Pure mullite's maximum high temperature strength is at 1500°C but, with impurities, that maximum strength can peak at temperatures below 1000°C.[32,35]

According to the phase diagram, the stoichiometry of mullite is not fixed at 71.8% alumina and 28.2% silica as given by $3Al_2O_3 \cdot 2\ SiO_2$. Rather, the composition of mullite as a solid solution is in the range from 70.5 to 74 wt% alumina.[30] (See Figure 2.17.) Mullite with alumina contents above 74% can be formed but are metastable[40,42] and cannot be formed by a solid state reaction between alumina and silica. If mullite is formed in the alumina rich region, excess alumina is easily detected as isolated α-alumina grains. If mullite is formed in the silica rich region, then the excess silica (usually amorphous) is not as easily detected as it can form as isolated islands and/or be present at grain boundaries. For best mechanical properties, pure mullite, with no excess silica trapped at the grain boundaries, is desired.[39,41]

Mullite has been traditionally used as a refractory, but more recently has been investigated and used for optical, dielectric and structural applications. As a result, much work has gone into processing mullite. With the use of chemically synthesized powders and colloidal consolidation methods, single phase mullite can be produced in the temperature range of 1250-1500°C. Previously, mullite powders were processed into dense bodies by either hot pressing above 1500°C or pressureless sintering above 1650°C. The low temperature processing techniques allow pressureless sintering of mullite matrix composites.[32] Webb[14] processed fully dense mullite using colloidal processing techniques by coating alumina particles with silica particles in the stoichiometry of mullite in water, consolidating the particles by evaporation and pressure filtration, and then sintering the compacts without pressure at 1500°C. These low temperature processing techniques

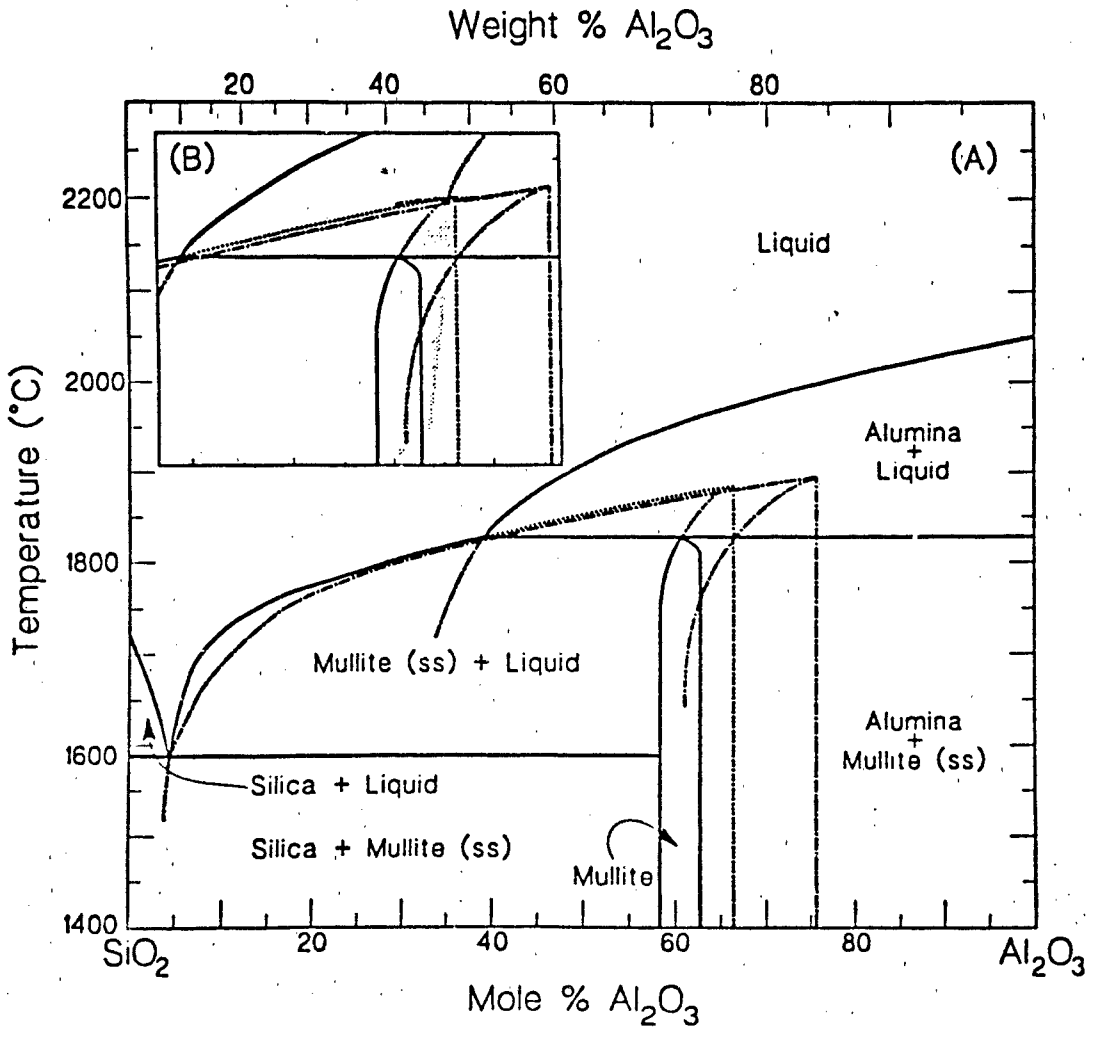

Figure 2.17 Phase Diagram of Al_2O_3 - SiO_2[31]

employ viscous phase (or transient viscous phase sintering) to attain densification before mullitization during the sintering process.

2.5 MULLITE COMPOSITES

Since mullite has such good high temperature properties, work has been done using mullite as a matrix and adding a second phase to improve on the fracture toughness. The majority of the work has involved hot pressing as the fabrication technique although recent work using viscous phase sintering has employed pressureless sintering techniques.[42]

The majority of the composite work accomplished has been adding mullite, SiC, or Si_3N_4 whiskers, ZrO_2 and SiC particles, and alumina platelets to a mullite matrix. The available mechanical properties of these systems are shown in table 2.2.[25,42]

Table 2.2 Mechanical Properties of Mullite Matrix Composites.

Dispersed Phase	Volume %	Strength (MPa)	Toughness $MPa \cdot m^{1/2}$
Mullite (w)	5	430	1.8
Mullite (w)	10	415	2.6
Si_3N_4 (w)	5	630	2.4
Si_3N_4 (w)	10	750	3.4
SiC (w)	10	422	3.6
SiC (w)	20	425	4.7
ZrO_2 (p)	15	400	4.5

The systems listed above (with the exception of the mullite-mullite composites) do not take full advantage of mullite's high temperature capabilities as most are good to a maximum temperature of 1200°C with drastic reduction in strength at higher temperatures. Further, with the exception of the ZrO_2 addition, all of the above systems were hot pressed to obtain >90% theoretical density.

Recent work by Sacks, et al.[43] shows that by using transient viscous sintering that densities of >95% of theoretical for a mullite/15% SiC system could be attained. Previous to this work, the only method to obtain reasonable densities in a particle reinforced mullite matrix was by hot pressing (except for the reaction sintering of alumina and zircon to attain mullite and zirconia).

Only the surface has been scratched with regards to mullite matrix composites. With increasing efficiency results obtained via colloidal and sol-gel processing techniques should allow for sintered densities close to theoretical. Additionally, depending upon the material application (such as grain size required, elimination of grain boundary and trapped silica, etc.) full densification, full mullitization and the interfacial bonding between the mullite and the reinforcing phase can be controlled via processing .

2.6 MOLYBDENUM DISILICIDE ($MoSi_2$)

$MoSi_2$ is a high melting point (2020°C) intermetallic most noted for its excellent resistance to high temperature oxidation.[2] This oxidation resistance at high temperatures (best of the silicides and almost as good as SiC) is due to the formation of protective SiO_2 layers on the surface of the $MoSi_2$. The silica coating is a non-spalling oxide which, once formed (above 900°C), keeps the base $MoSi_2$ protected at lower temperatures and during thermal cycling. This high temperature oxidation behavior is governed by the reaction:[44,45]

$$5MoSi_2 + 7O_2 \rightarrow Mo_5Si_3 + 7\ SiO_2 \quad \text{(see Figure 2.18)}$$

Once the layer is formed, further oxidation is limited because of slow diffusion through the existing oxide layer.[44] The Molybdenum - Silicon phase diagram (Figure 2.18) shows that as silicon is removed the progression is from $MoSi_2$ to Mo_5Si_3.

Currently, the most wide spread use of $MoSi_2$ is as electric heating elements for high temperature (~1900°C) furnaces.[46] Its hot corrosion resistance is also an order of

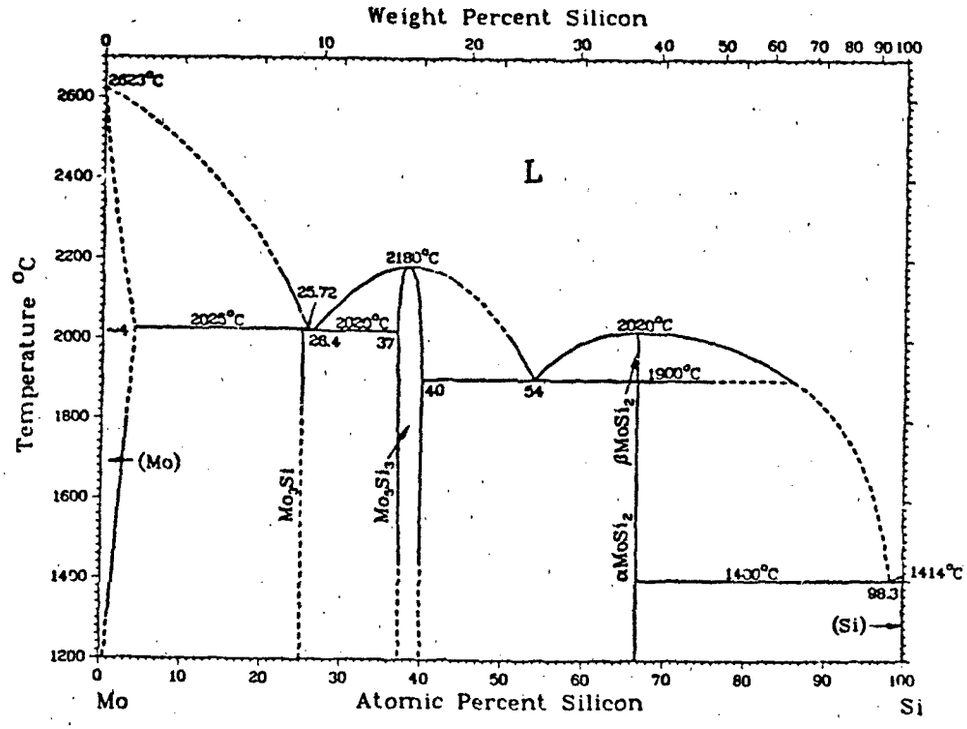

Figure 2.18 Phase diagram of Mo - Si

magnitude better than that of the best nickel based alloys. Additionally $MoSi_2$ undergoes a brittle to ductile transition at ~1000°C.[44]

However, as with most intermetallics, $MoSi_2$ suffers from mechanical property deficiencies such as low ductility at temperatures below its brittle to ductile transition point, and poor strength and creep resistance above 1250°C.[44] $MoSi_2$'s properties suggest that it could be used as a reinforcing particle in a composite giving improvements in high temperature mechanical properties such as fracture toughness, strength, and crack growth behavior of the matrix while, at the same time, improving low temperature characteristics by the various toughening mechanisms described earlier.[47]

Work has been accomplished using $MoSi_2$ both as a matrix and as a reinforcing phase to explore its potential as a high temperature material for use in gas turbine engines. Mechanical testing has been performed on $MoSi_2$ in conjunction with SiC, Si_3N_4, Partially Stabilized ZrO_2, and WSi_2 with results listed in table 2.3.[44,47-49]

Table 2.3 Properties of $MoSi_2$ and $MoSi_2$ Composites.

Matrix	Reinforcement (Particles)	Strength (MPa)	K_{Ic} ($MPa \cdot m^{1/2}$)	Temperature
$MoSi_2$ (pure)	NA	150	5.3	Room
$MoSi_2$	ZrO_2 (30 vol%)		6.6	Room
50/50mol% $MoSi_2/WSi_2$	SiC (20 vol%)	590	--------	1200°C
	(15 vol%)	150	--------	1400°C
	(10 vol%)	80	--------	1500°C
$MoSi_2$	SiC (20 vol%)	310	8.2	Room
Si_3N_4	$MoSi_2$(20vol%)	275	--------	1200°C
	(10vol%)	120	--------	1500°C

Additionally, oxidation experiments were accomplished with: (1) $MoSi_2$ as a matrix with additions of TiB_2, ZrB_2, HfB_2, and SiC,[44] and with (2) $MoSi_2$ as a reinforcing phase in a mullite, alumina and strontium alumina disilicate matrices.[4] Results in the first study

indicate that the $MoSi_2$-SiC system has the best oxidation resistance in terms of the least weight gain and best adherence of the SiO_2 protective layer. Results from the second study determined that mullite is an "appropriate host for oxidizable silicon containing phases" which would imply that $MoSi_2$ particles would work in a mullite matrix.

In porous $MoSi_2$ compacts (or porous composite compacts containing $MoSi_2$) low temperature (<800°C) oxidation is a serious problem. The reaction that takes place does not form a protective layer and is governed by:[44,45]

$$2MoSi_2 + 7O_2 \rightarrow 2MoO_3 + 4\ SiO_2$$

with the MoO_3 as a gas. When this low temperature oxidation occurs, the $MoSi_2$ disintegrates (commonly called "pesting"). This reaction only occurs in porous $MoSi_2$ bodies so with proper processing to attain relatively dense bodies, this pesting is not a problem (as indicated by the wide spread use of $MoSi_2$ as heating elements in oxygen furnaces).[44]

2.7 TESTING OF MECHANICAL PROPERTIES OF CERAMICS

There are several mechanical properties that can be determined including: tensile strength, flexure strength, shear strength, fracture toughness, elastic moduli, work of fracture, impact resistance, and fatigue behavior to name a few. Since the primary objective of this work is to improve the toughness of the mullite - $MoSi_2$ system relative to that of monolithic mullite, only fracture toughness and strength will be measured.

2.8 STRENGTH

The tensile strength of ceramics is usually measured experimentally by three or four point bend tests (see Figures 2.19, 2.20). In three point bending the peak stress occurs along a line on the specimen face opposite the central applied load. In four point bending

the peak stress occurs over an area between the two internal applied loads which allows for a greater chance of a critical flaw to be exposed to the peak stress. This results in four point bend strength values that are less than three point bend strength values but also more reliable as a greater portion of the material is exposed to the peak stress. In both cases, the advantage is the tests' simplicity: the specimen has a simple form (rectangular beam) and no grips need to be attached. In four point bending, strength is determined by:[50]

$$\sigma_f = \frac{3\,Fa}{2\,bd^2}$$

Equation 2.28

2.9 FRACTURE TOUGHNESS

The predominant method of testing toughness (or critical stress intensity factor, K_{Ic}) in ceramics is through the use of the single edge notched beam (SENB) test (see Figure 2.21). This test is accomplished similarly to the three point bend test, but the test specimen is notched and the notch is placed directly opposite the applied load. The same advantages apply as to strength testing, however, a limitation of this type of specimen is that once fracture is initiated, the ceramic specimen almost invariably breaks into two pieces, and thus only the fracture energy to initiate a crack can be estimated. For good experimental results, three requirements must be met: (1) the size of any plastic zone near the tip of the crack is sufficiently small to be negligible, (2) the specimen dimensions must be large when compared to the microstructural features of the material, and (3) the crack or notch should be atomically sharp at its tip. The first requirement is not critical except at high temperatures when plastic effects in ceramics are more pronounced. The second requirement presents little problem except in coarse structured materials. The third requirement is critical but, in most cases, the machining operation which produces the notch leaves a sufficiently sharp crack at the end of the notch (see Figure 2.22).[50] Brown and Srawley derived the relation for determining K_{Ic}:[54]

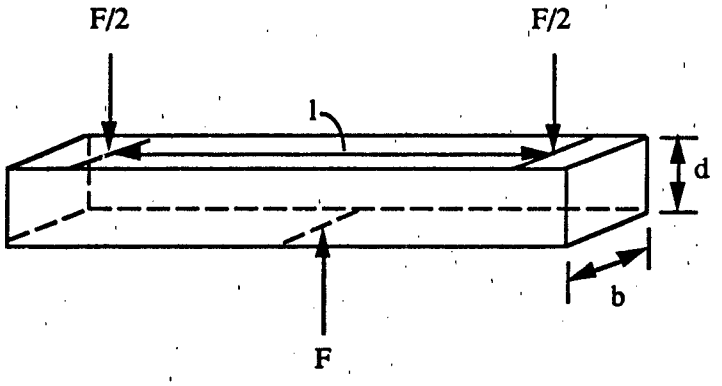

Figure 2.19 Three point bend test (with critical dimensions).

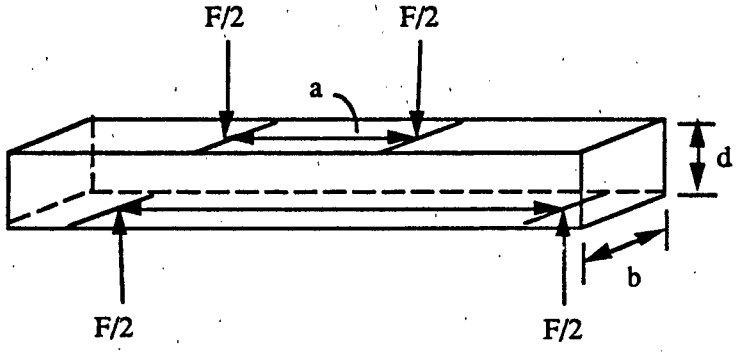

Figure 2.20 Four point bend test (with critical dimensions)

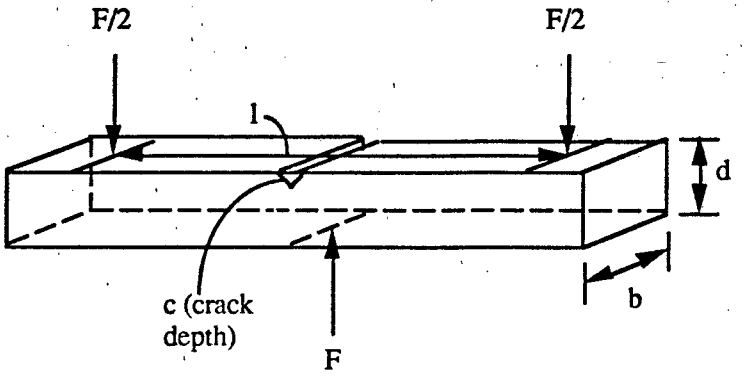

Figure 2.21 Single Edge Notched Beam (SENB) (with critical dimensions)

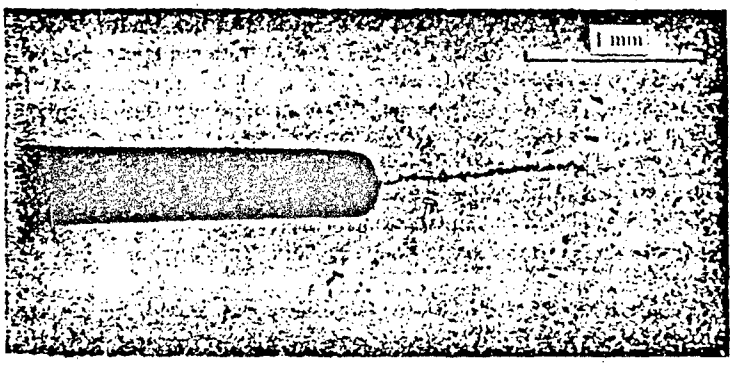

Figure 2.22 Sharp crack at the tip of a specimen notch [51]

$$K_E = \frac{3Flc^{1/2}}{2bd^2}\left[F\left(c/d\right)\right]$$

Equation 2.29

where F(c/d) is a polynomial function related to c/d.

CHAPTER 3

EXPERIMENTAL PROCEDURES

As stated in the goals of this research, essentially two studies took place in this research: (1) to investigate the possibilities of using a mullite matrix - $MoSi_2$ particle reinforced system for high temperature applications and (2) to investigate the potential of pressureless sintering the mullite-$MoSi_2$ composite by transient viscous phase sintering.

3.1 MATERIALS AND CHEMICALS

The alumina powders used in this study were AKP-50 and AKP-G (both from Sumitomo Chemical Company, Japan). AKP-50 is a high purity α-alumina (≥99.995%) with an average particle size of 0.24 μm and a specific surface area of 9.5 m^2/g. Over 90% of the powder was particles between the sizes of 0.1 - 0.3 μm. AKP-G is a high purity γ-alumina (≥99.99%) with particle size less than 0.1 μm and a surface area of 150 m^2/g. No particle size distribution was supplied by the manufacturer.

The silica used in this study was LUDOX-AS colloidal silica provided by E. I. duPont de Nemours and Company (Wilmington, DE). LUDOX-AS is an aqueous colloidal dispersion of silica particles consisting of discrete uniform spheres of amorphous silica. The stabilizing counter ion in the LUDOX-AS is ammonium and the LUDOX-AS was stable in the as received pH of 9.5. As stated in the manufacturers literature, the average particle diameter is 22 nm, specific surface area of 140 m^2/g and consists of 40 wt% silica. Small amounts of impurities (as a result of the precipitation preparation process) consisted largely of sodium. Previous work [52] showed that the particle size was 160 Å (TEM analysis) not the 22 nm as stated in the manufacturer's literature.

The $MoSi_2$ powder was provided by Atlantic Equipment Engineers (Bergenfield, NJ). The manufacturer's literature stated that it was 99.8% pure, was insoluble in water

and had a density of 6.2. The as-received powder was said to have a particle size distribution of 1-5 μm, but this was not confirmed during SEM analysis. Rather the particles were ≤40 μm in size with the larger particles being rod-like in shape (see Figure 3.1).

(Initial research used a mullite powder precursor obtained from Seattle Super Conductor (SSC) that, when heated to 1400°C, would convert to mullite powder. No further information is provided as it was used to establish phase stability between the mullite and the $MoSi_2$ and was not used in the rest of the study. The initial $MoSi_2$ powder (provided by CERAC, Milwaukee, WI) was also used during the phase compatibility study and not during the remainder of the research.)

1.0 N solutions of HNO_3 and NH_4OH for use in controlling the colloidal behavior of the alumina and silica particles were prepared from concentrated solutions diluted with deionized water. All suspensions were made using deionized water.

The glassware used in these experiments was standard Corning Pyrex. Prior to use the glassware was washed in tap water and rinsed with deionized water. Extreme care was not taken in removal of impurities from the glassware as the solids loadings were deemed large enough to render any impurities insignificant.

3.2 PHASE STABILITY/COMPATIBILITY

Before further work could be accomplished, the phase stability/compatibility of mullite and $MoSi_2$ had to be determined. Mullite powder (SSC) and $MoSi_2$ (CERAC) were mixed dry using a diamonite mortar and pestle, dry pressed (7500 psi), and then heated to 1500°C and held for two hours, 15 hours and 100 hours. An additional test was performed by hot pressing (Elatec, Woburn, MA) a sample using the above two powders,

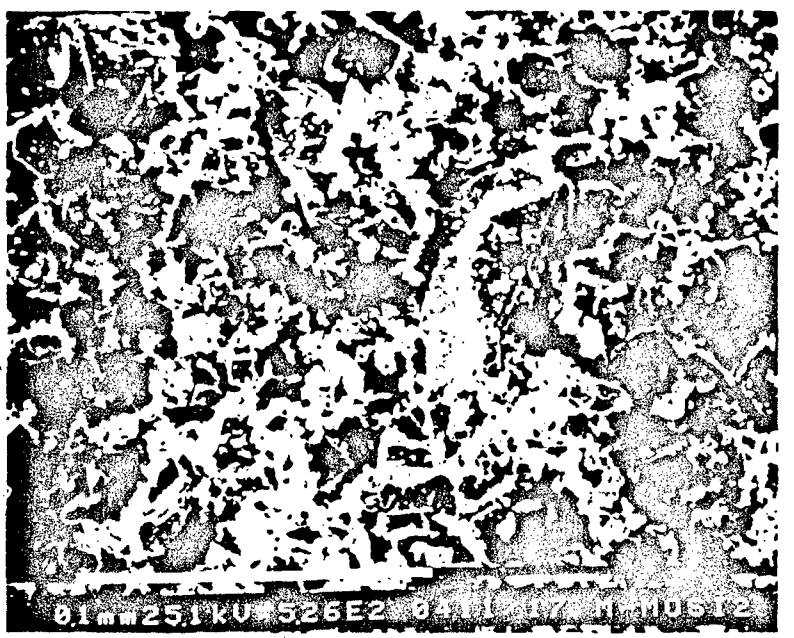

Figure 3.1 As received $MoSi_2$ powder.

this time mixed in 100% pure alcohol, dried, packed in grafoil in the hot press and pressed to 10,000 psi at 1650°C.

3.3 PREPARATION OF SUSPENSIONS

In order to make the mullite precursor - $MoSi_2$ solution, the AKP-50 (α-alumina), AKP-G (γ-alumina) and LUDOX-AS (silica) had to be prepared in suspension form.

α-alumina was mixed in deionized water at a solids loading of 8.8 vol%. Such a low solids loading (AKP-50 can easily be prepared at up to 40-50 vol% or greater in water with steric aids) was for more effective classification by sedimentation. About 210 grams of α-alumina was mixed into ~600 ml of deionized water. Throughout the mixing the pH of the suspension was maintained at 3.5 with periodic additions of the 1.0 N HNO_3 solution. After the addition of ~100 grams (or half of the α-alumina), the suspension was ultrasonicated to break up agglomerates. Three of these batches were made for a total of ~2 liters of stock α-alumina solution. This stock solution was sedimented for three days to remove any large agglomerates or particles. The supernatant was then poured off and kept on a stir plate until used. The supernatant's solids loading was in the range of 6.8-7.8 vol% after the sedimentation process. Solids loading was determined by weighing a porcelain crucible dry, pouring the suspension into it, weighing it full, heating it to remove the water, then weighing the dried powder containing crucible and comparing measurements.

γ-alumina was prepared in essentially the same way as α-alumina with one exception. Since the surface area of the γ-alumina is much greater than that of α-alumina, suspensions were more difficult to prepare. As a result, lower solids loading was used to make the suspensions. Two batches of 90 grams of γ-alumina were added each to 500 ml

of deionized water (4.7 vol% solids loading) to form a total of ~1 liter of suspension. After sedimenting for 2 days, the solids loading in the supernatant was reduced to 2.2-2.9 vol%.

LUDOX-AS was prepared by mixing the as-received suspension with equal parts water for two reasons: (1) to prevent precipitation of the silica on the sides of the beaker glass and (2) to better control the pH. LUDOX-AS was received at pH 9.5; adding an equal part of deionized water lowered the pH to 9. The pH was then adjusted to 3.5 with the 1.0 N HNO_3 solution.

Because the $MoSi_2$ particles were so large with respect to the alumina and silica particles, the $MoSi_2$ was mixed into deionized water, ultrasonicated, and then classified by sedimentation for a period of 40-80 minutes (see Figure 3.2). After sedimentation, the supernatant was dried resulting in a 15-20 wt% return on the amount of powder mixed in the deionized water prior to sedimenting. The remaining dried powder was ground in a diamonite mortar and pestle and mixed again in deionized water (at about a 10 vol% solids loading) and ultrasonicated. This remixing in water resulted in better mixing when combined with the alumina-silica suspension. Various amounts of $MoSi_2$ were added depending on the desired final product composition (2.5, 5, 10, 15 and 20 vol% $MoSi_2$ in the mullite matrix).

Previous work by Webb[14] determined that for the final mullite product, the alumina should consist of 90.54% α-alumina and 9.46% γ-alumina. Additionally, it was determined that the separate suspensions of α-alumina and γ-alumina should be mixed separately with the LUDOX-AS and then combined with the final product being 71.8% alumina and 21.8% silica. This was done to ensure complete coating of the alumina particles by the silica particles. The amount of silica mixed with each type of alumina was determined by the specific area of each alumina powder with total amount used adding up to the 21.8%.

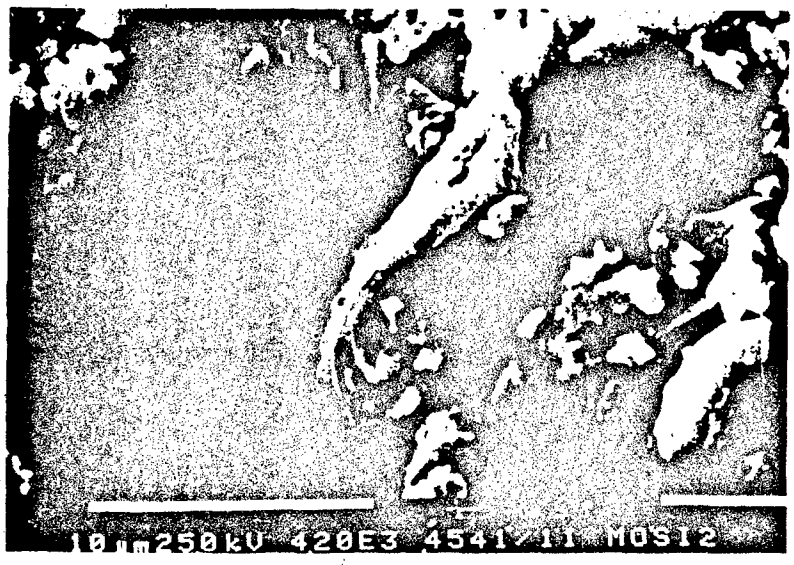

Figure 3.2 $MoSi_2$ powder after sedimentation

α-alumina was mixed with silica at pH 3.5, γ-alumina was mixed with silica at pH 3.5, and then the two suspensions were mixed. At this point one of two steps was taken. Either the suspension was left at pH 3.5 and the $MoSi_2$ in deionized water was added, or the $MoSi_2$ in deionized water was added and the suspension's pH was changed to 10 by addition of the 1.0 N NH_4OH. The pH was changed to 10 because that resulted in the best sintered density for pure mullite.[14]

Once all of the ingredients were combined, concentration of the suspension took place. Concentration occurred by evaporating the water out of the suspension on a hot stir plate until the total volume of the system was reduced by approximately 2/3 (or just enough liquid for the suspension to still stir on the stir plate). The suspension was then cooled.

The above processing steps (minus the addition of the $MoSi_2$) were determined to be the optimum method (with changing the suspension to pH 10 slightly favored over keeping the system at pH 3.5) for processing dense mullite due to the effective heterocoagulation of the alumina and silica particles (silica coating alumina) and then keeping the silica coated alumina particles separate for densest packing upon consolidation.[14]

3.4 PRESSURE FILTRATION

In order to speed up the consolidation process and to reduce cracking caused by shrinkage, pressure filtration was chosen to consolidate the composite slurry. Figure 3.3 shows a schematic of the pressure filtration apparatus. The apparatus consisted of a transparent polycarbonate piston and cylinder with the pressure provided by a gas (argon or helium) to drive the piston into the slurry. Water was then removed through a disposable 0.1 μm filter, which was supported by either a 0.5 μm stainless steel filter or a cloth filter and then both configurations were further supported by a porous teflon circular block. The

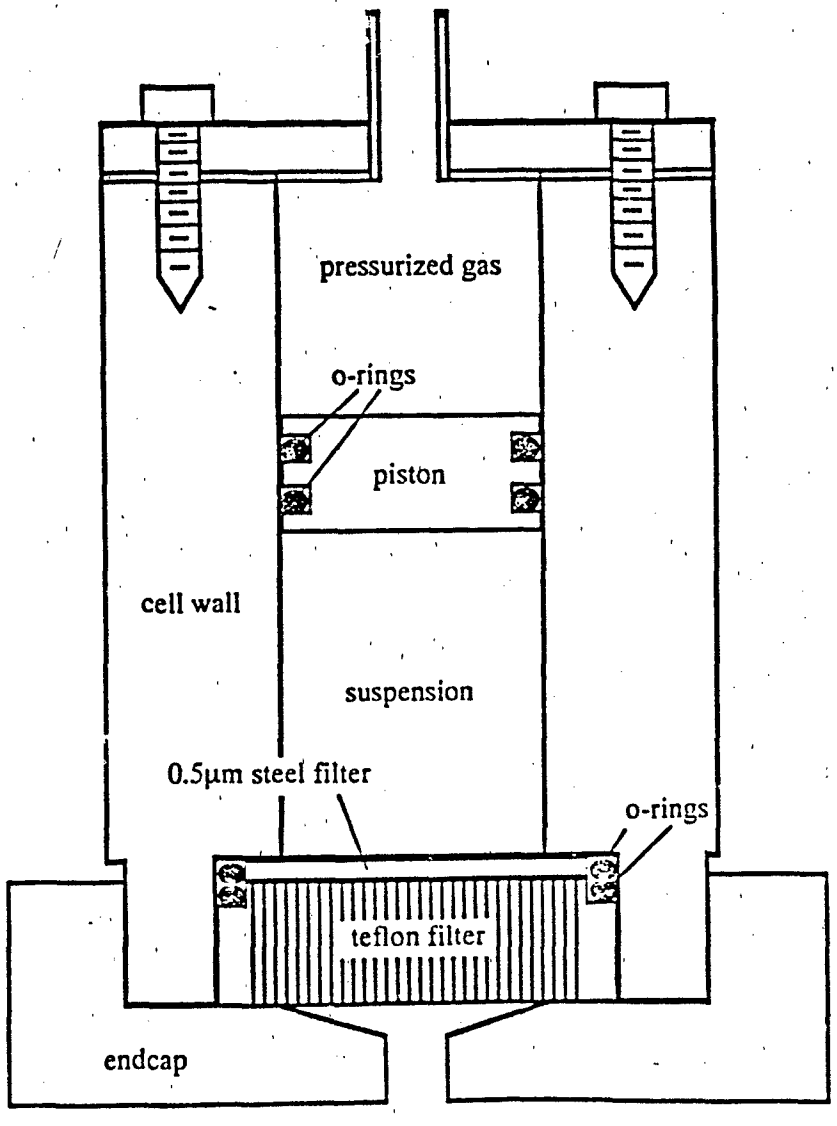

Figure 3.3 Pressure filtration apparatus (not to scale). Bore of the cylinder was either 1.5 or 3 inches depending on the type of sample desired.

array of filters were held on by a PVC end cap with a hole through which the water could pass. A brass plate with a Swageloc fitting was sealed to the top of the cylinder by 1/4 inch bolts. All parts were machined with the exception of the filters and the standard 0-rings used as seals.

After the slurry underwent evaporation and cooling, it was poured into the cylinder. Any trapped bubbles were removed mechanically (by shaking the container against a table and by using a spatula) as the majority of bubbles would stick to the cylinder walls or plunger. The gas pressure was slowly increased to a pressure of 3.5 MPa controlled by a standard regulator. The filtration time varied depending on the amount of slurry used, the type of cylinder used and the amount of $MoSi_2$ that was added. The end point of the filtration was determined visually by checking the water flow through the filters and by observing the plunger's progress into the slurry.

3.5 DRYING AND SINTERING

Pressure filtered samples were dried in one of two ways: (1) at room temperature for two or more days, or (2) at room temperature for one to two days, then one day in a 50°C forced air drying oven. Drying was to ensure that the samples would not crack during sintering in the furnace.

Those samples that were for density tests were cut into four to six pieces and sanded to ensure more accurate measurements. Samples destined for mechanical testing were sanded to flat, parallel sides (mainly to remove the filter imprint from the sample) and cut to fit into the Cold Isostatic Press (CIP). The samples that were to be hot pressed were crushed and ground into a powder using a diamonite mortar and pestle.

Cold isostatic pressing (Autoclave Engineering Inc., Erie, PA) was used on all pressureless sintered samples. Pressures of 350 MPa (50 ksi) for times of five minutes

were used after putting the samples in evacuated latex bag (condoms) to prevent contamination of the green compacts by the oil-water medium in the CIP.

Sintering was accomplished in one of three ways depending upon the sample used:

a. pure mullite was sintered in an ambient atmosphere furnace (Model 51314, Lindberg, Watertown, WI) at a temperature of 1500°C for six hours.

b. Pressureless sintered mullite - $MoSi_2$ composites were sintered in an argon atmosphere, graphite furnace (ASTRO, Model 2570, Santa Barbara, CA) at temperatures ranging from 1500°-1530°C for four hours.

c. Hot pressed samples were sintered in a vacuum environment, graphite die and furnace hot press. It consisted of a uniaxial press which was manually controlled from 0-23 MPa in pressure. Samples were sintered at 1500°-1600°C for two hours at the maximum pressure. Pressure was initially applied at 1000°C and gradually increased to the maximum at 1300°C. The reason that the maximum pressure was reached below the sintering temperature was that Webb[14] determined that, for pure mullite, densification occurs at 1300°C after which mullitization takes place at the higher temperature.

Additionally, some samples were heated in the ASTRO furnace to 1300°-1320°C, cooled and removed, heated again to 1300°-1320°C in the Hot Isostatic Press (Model SL-1 Mini-HIPper Laboratory Press, ASEA Pressure Systems, Columbus, OH) at 210 MPa, cooled and removed, and then sintered at 1525°C in the ASTRO furnace. All composite samples were placed in alumina crucibles totally surrounded by and packed in $MoSi_2$ powder.

A processing flow chart (Figure 3.4) depicts the processing procedure from start to finish.

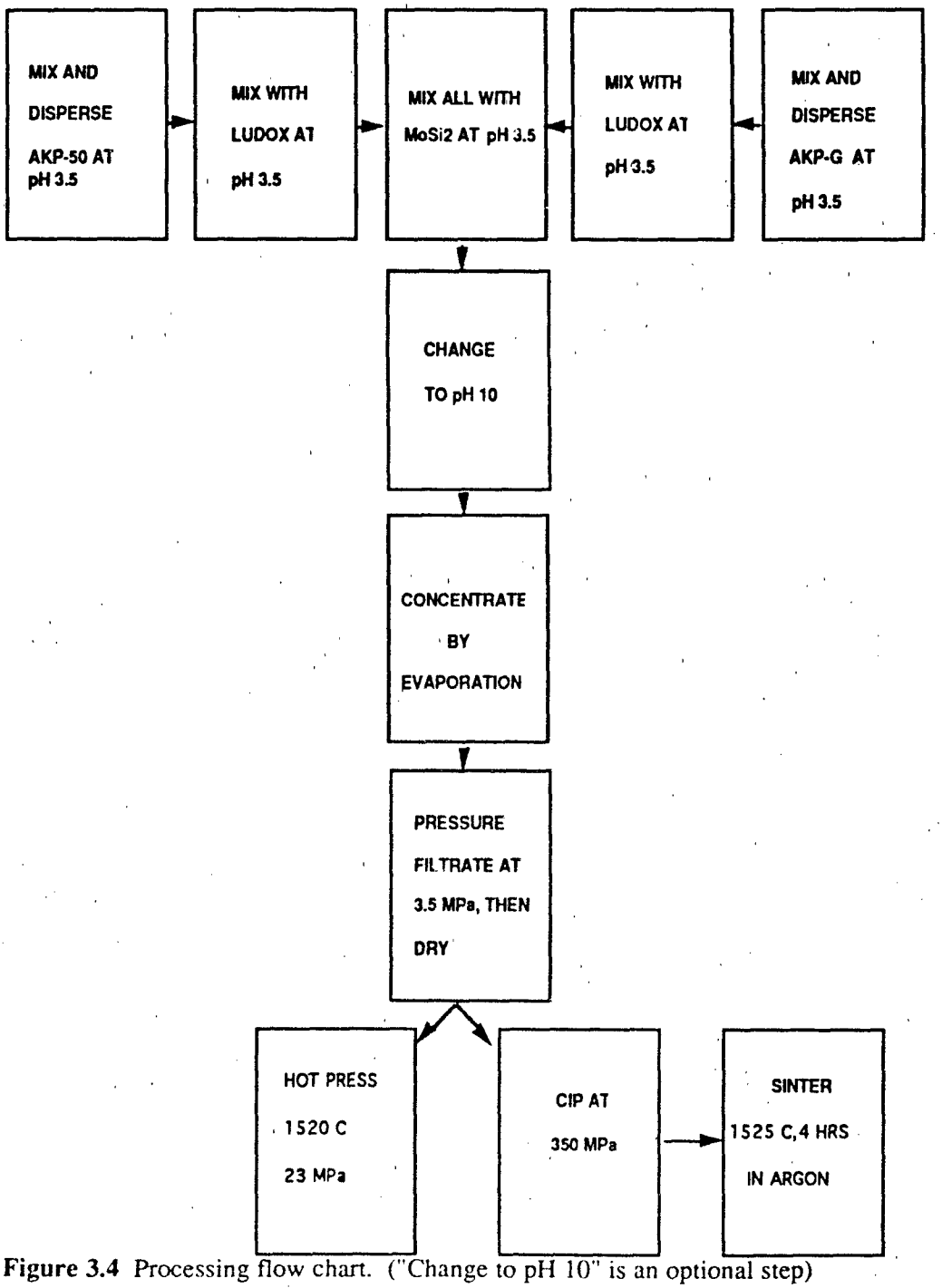

Figure 3.4 Processing flow chart. ("Change to pH 10" is an optional step)

3.6 CHARACTERIZATION

3.6.1 DENSITIES

Green and sintered samples were measured to obtain their densities using the Archimedes technique according to the ASTM standard.[53] Green samples were measured in kerosene as the liquid medium. Sintered samples were measured using deionized water as the liquid medium.

3.6.2 X-RAY DIFFRACTION

Phase identification was accomplished using x-ray diffraction (X-Ray Diffractometer, Philips Electronic Instruments, Inc., Mahwah, NJ) on sintered and densified samples. Samples were crushed in either a diamonite mortar and pestle or by using a hammer imparting force on a stainless steel plunger into a stainless steel cylinder. The 2θ range was 15-70°, operating voltage was 45 kV, operating current was 40 mA, and the scan increment was 0.025° 2θ for 0.25 seconds.

3.6.3 MICROSCOPY

Optical microscopy (Leitz Metallovert Microscope, Germany) was used on polished and fractured surfaces. Scanning electron microscopy (SEM) (SEM515, Philips, Holland) was used in the characterization of the sintered samples, oxidized samples, the fracture test specimens and the indented samples. All were observed at an operating voltage of 25 kV. Sintered samples were polished down to 0.3 μm alumina powder after which they were either viewed in the SEM or oxidized and then viewed, or indented and then viewed. Fracture specimens were cut using a low speed saw (Buehler Isomet Low Speed Saw, Evanston, IL). All specimens were sputter coated with a coating of gold-palladium.

3.6.4 TESTING OF MECHANICAL PROPERTIES

Samples were surfaced and sliced (diamond wheel and blade) (DoAll Microtomatic Slicing Machine MTM-612, Des Plaines IL) to form approximately 2.5 x 2.5 x > 43 mm test specimens. Samples destined for strength testing were polished (to 0.3 μm alumina powder) on the face opposite the applied load and then subjected to four point bending as described by Davidge.[51] The outer span size was 38.1 mm and the inner span size was 12.7 mm. The critical stress intensity factor (K_{Ic}) was determined using the single edge notched beam (SENB) test in three point bending.[54] The notch was also cut using the DoAll slicer. Both tests were performed on the INSTRON Universal Testing Machine (INSTRON UTM Models 4505, 1122, Park Ridge, IL) with a cross head speed of 0.05 mm/min.

CHAPTER 4

RESULTS AND DISCUSSION

4.1 PHASE COMPATIBILITY AND PROCESSING

Prior to proceeding with this work, verification had to be made that $MoSi_2$ particles would not react with the mullite matrix to form any unwanted phases during sintering and subsequent oxidation. Mullite (SSC) powder was mixed with $MoSi_2$ in a 50/50 vol% ratio, dry pressed, then heated to 1500°C in an ambient atmosphere for 2 and 15 hours. X-ray diffraction (XRD) analysis showed no phases combining the $MoSi_2$ and mullite. What was discovered, however, was that the mullite peaks remained stable regardless of the heating time, the $MoSi_2$ peaks slowly disappeared, and Mo_5Si_3 peaks appeared. This can be explained using the Molybdenum-Silicon phase diagram (Figure 2.18) and the internal oxidation that was discussed in Section 2.6.

It was now known that mullite and $MoSi_2$ were non-reactive with each other (as far as characterization by x-ray diffraction shows). Since Borom, et al.[4] were the only group to fabricate a mullite-$MoSi_2$ sample, verification was needed to determine that a sample could be made with the powders on hand. The mullite and $MoSi_2$ (20 vol%) powders were mixed in alcohol, dried, ground with a mortar and pestle and loaded into the hot press. Hot pressing was accomplished at 1650°C with 69 MPa applied pressure in vacuum for two hours. XRD analysis (see Figure 4.1) showed mullite and $MoSi_2$ as the only crystalline phases present. SEM analysis also showed distinct $MoSi_2$ particles in the mullite matrix.

After determining that mullite and $MoSi_2$ could be formed into a composite, an attempt was made to hot press a rectangular billet of the 20 vol% $MoSi_2$ composite. During the hot pressing cycle, the press failed shattering the graphite die, plungers and heating elements. At that time it was determined to attempt to fabricate the composite using

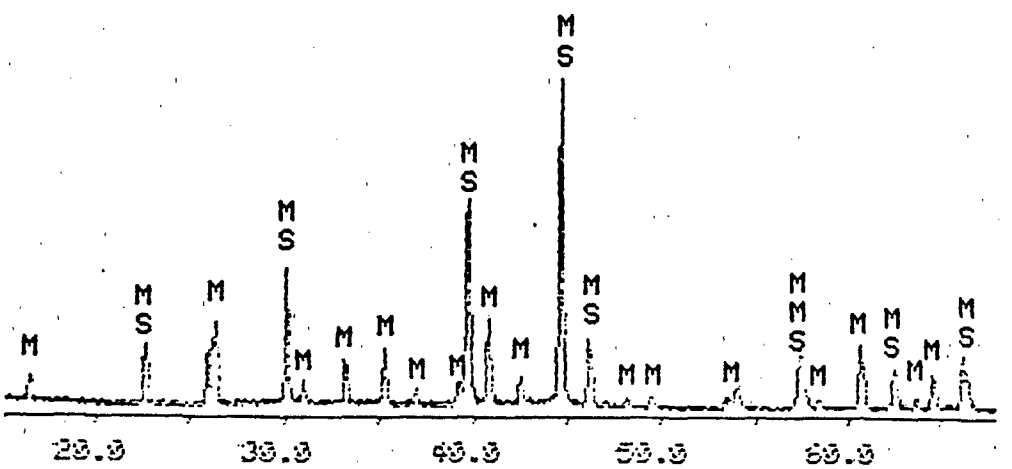

Figure 4.1 Initial hot pressed sample (SSC mullite powder, -325 mesh $MoSi_2$ powder)

the pressureless sintering techniques that were developed by Webb,[14] to make mullite, and then add the $MoSi_2$ to the suspension prior to consolidation.

20 vol% $MoSi_2$ was added to the alumina-silica suspension, consolidated by evaporation, pressure filtrated, dried and then sintered in ambient atmosphere at 1600°C for six hours. The results showed that the composite could not be sintered in air. At fast heating rates (≥ 20°C/min), a good portion of the $MoSi_2$ remained, but, Mo_5Si_3 was also present (and amorphous silica). At slower heating rates (5°C/min) all that was left after "sintering" was white mullite powder loosely held together. What was exhibited during this phase of the study (and during the initial tests described earlier but not realized at that time) was the "pesting" or internal oxidation of the $MoSi_2$ that occurs in porous bodies. The silicon was converting to amorphous silica as determined earlier, but the molybdenum was volatilizing as MoO_3 which appeared as a yellow film on the alumina crucible covering the sample.

The next attempt at sintering was by packing the composite in $MoSi_2$ powder under the assumption that the $MoSi_2$ powder would react with the oxygen in the furnace during sintering and thus act as an oxygen getter. The $MoSi_2$ powder did react as expected but so did the $MoSi_2$ in the sample that was to be sintered. After this it was determined that the composite could not be sintered in air.

Sintering under high vacuum (10^{-4} - 10^{-5} torr) was tried next to stop the $MoSi_2$ from oxidizing. Samples were sintered both packed in $MoSi_2$ and exposed to the vacuum in the ASTRO furnace. While the results were better, a very porous scale formed on the outside of the sample anywhere from 0.5-2 mm thick. This scale, consisting of Mo_5Si_3 (Figure 4.2), mullite, alumina and $MoSi_2$ was believed to be formed by reaction of the silicon with the graphite in the furnace to form SiC. Further characterization is needed to determine exactly what was happening. An argon atmosphere was used next for sintering

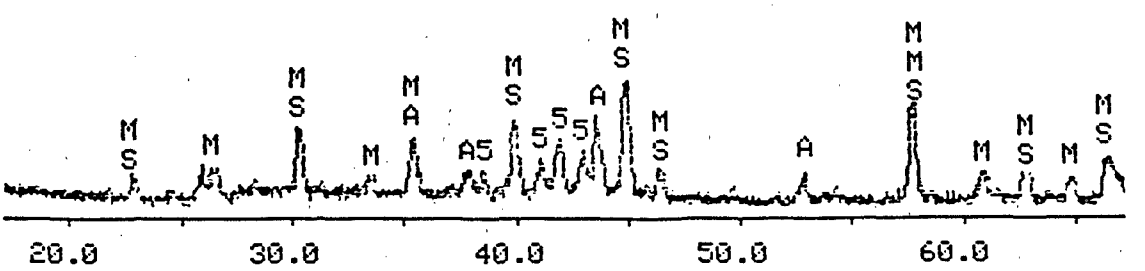

Figure 4.2 XRD pattern of scale (M = mullite, MS = $MoSi_2$, 5 = Mo_5Si_3, A = Alumina)

the composite both packed and unpacked in $MoSi_2$. The sample which was not packed in $MoSi_2$ showed the same porous scale as the composite sample sintered in a vacuum, but the sample packed in $MoSi_2$ formed no scale, and when XRD analysis was performed, only mullite and $MoSi_2$ were present. Figure 4.3 shows the XRD patterns of the mullite matrix and 5, 10, 15 and 20 vol% $MoSi_2$ reinforcement.

After this portion of the study, it was realized that samples could be made in the hot press, and that the pressureless sintering technique was to sinter the composite sample in an alumina crucible packed in $MoSi_2$ powder.

4.2 PROCESSING

Successful low temperature (≤1600°C) pressureless sintering of high density mullite matrix composites is a relatively new process.[34] Previous work routinely required hot pressing or pressureless sintering at temperatures ≥1650°C to attain reasonable densities without excessive shrinkage or warpage. Sol-gel techniques, while providing ≥98 % dense pure mullite experienced much lower relative densities when sintered with Si_3N_4 particles or SiC whiskers -- with densities dropping to 90% and 85% respectively for 15 vol% loadings. Use of transient viscous phase sintering to aid in composite densification by combining alumina and silica (silica as the transient viscous phase) is a key to the pressureless sintering of mullite matrix composites.

This study used the procedure developed by Webb[14] to process the mullite matrix. The $MoSi_2$ particles were added to the alumina-silica suspension at pH 3.5 and either maintained at that pH or the pH was changed to 10. Since this method of processing mullite used electrostatic stabilization in the suspension, it was important to learn the surface charge characteristics of the $MoSi_2$ particles when dispersed in water. After testing the surface charge of the particles across most of the pH spectrum using a zeta meter (Mark

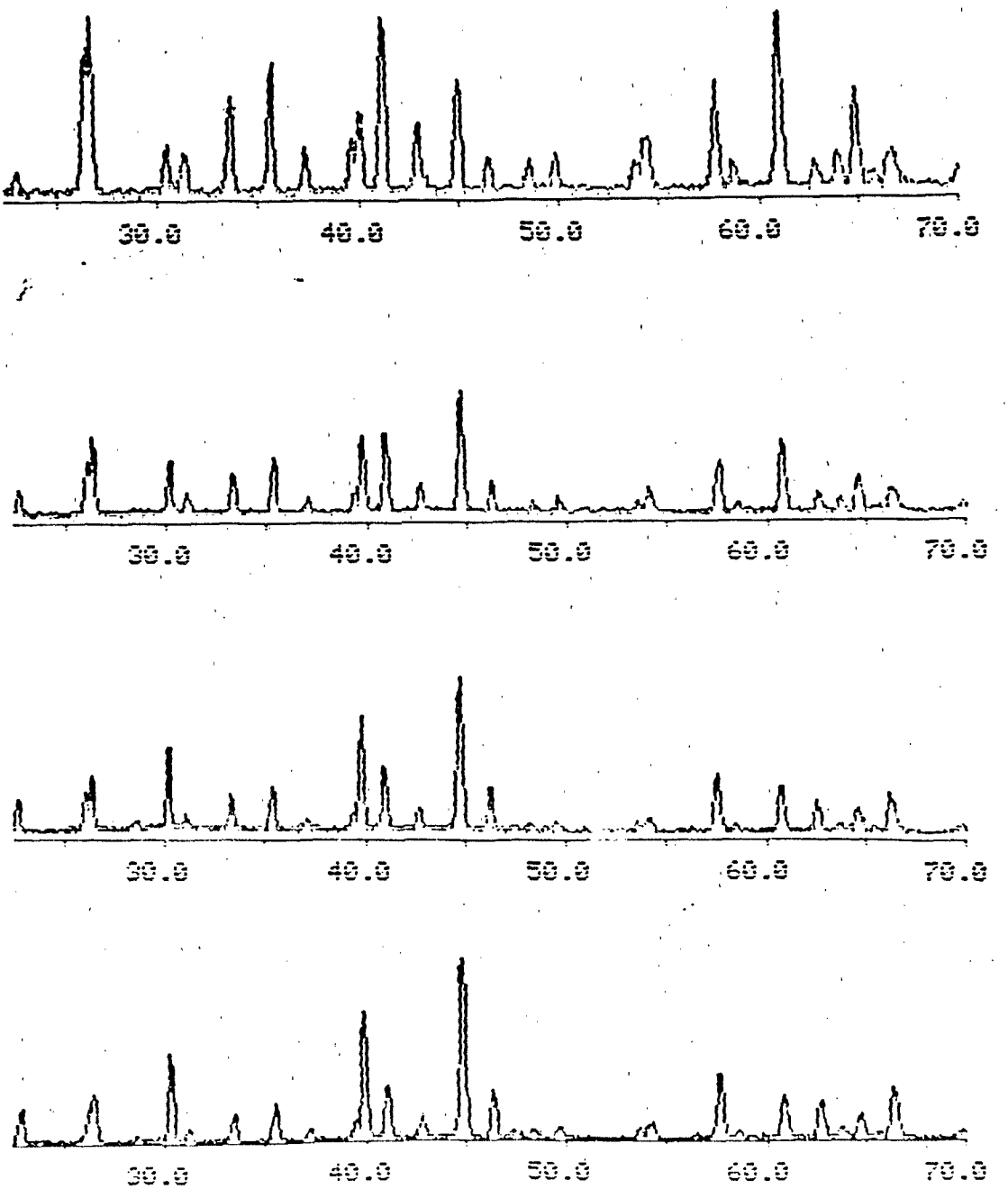

Figure 4.3 XRD patterns of (from top): 5 vol% $MoSi_2$, 10 vol% $MoSi_2$, 15 vol% $MoSi_2$, and 20 vol% $MoSi_2$

II, Rank Brothers, England), it was established that $MoSi_2$ had a positive ζ potential (surface charge) at pH 3.5 and at pH 10 (ζ potential of ~25 mV at pH 3.5 and ~51 mV at pH 10).

To test what difference varying the pH would make, samples were prepared (suspensions mixed, evaporated, pressure filtered, dried, CIP'ed and sintered) at both pH 3.5 and at pH 10. The results (Figure 4.4) show that at low concentrations of $MoSi_2$ (up to 10 vol%) there was negligible difference in sintered densities between the two methods. This may be explained somewhat by percolation theory -- that once a critical volume % of inclusions is reached, bulk densification will be slowed down or stopped.[43] In addition, at lower concentrations, there exists a smaller portion of large particles, so there is less chance of large pores forming around large particles. However, at the higher concentrations of $MoSi_2$ (15 and 20 vol%) there was a noticeable difference in sintered densities. It is hypothesized that: (1) percolation theory as described above applies, (2) due to stronger attractive forces between the silica coated alumina particles at pH 10 then pH 3.5, the $MoSi_2$ particles were being coated by the alumina-silica particle systems, and/or (3) while raising the pH from 3.5 to 10, the system flocculates at ~pH 5-7, then deflocculates at a higher pH (~pH 8.5) but does not totally deflocculate. The first case is what is hoped to be avoided by using viscous phase sintering, but in both of the other cases, agglomerate rather than particle packing is achieved resulting in lowered sintered densities.

Webb[14] showed that the attractive forces between the alumina and silica were strong enough that even ultrasonication did not provide enough shear force to totally break up the silica coated alumina particles. When the system is a pH 10, the silica coated alumina particles' surface charges are strongly negative which in Webb's[14] work led to a dispersed system. However, with additions of positively charged $MoSi_2$ particles, strong attractive forces between the $MoSi_2$ particles and the silica coated alumina particles would

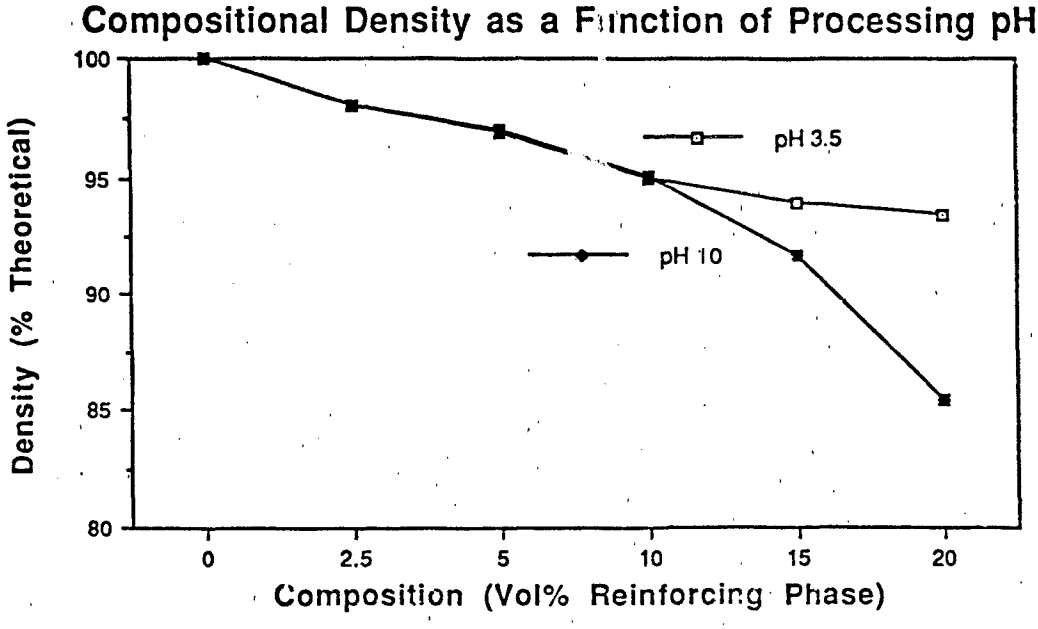

Figure 4.4 Comparison of sintered densities of mixing at pH 3.5 and pH 10.

seem to occur (not checked experimentally) leading to agglomeration. At pH 3.5, where alumina is positive, silica is negative and $MoSi_2$ is positive, the attraction would not be as strong.

Figure 4.5 shows SEM micrographs of a 15 vol% $MoSi_2$ composite processed both at pH 3.5 and at pH 10. Note the size of the pores around the larger $MoSi_2$ particles in the sample processed at pH 10. These are felt to be caused by agglomerate packing. The sample processed at pH 3.5 does still have a substantial amount of uniform, small porosity which could be a result of smaller agglomerate packing due to the hypothesized weak attractive forces between the $MoSi_2$ and silica coated alumina particles. It is felt that if smaller particle sized inclusions (this study used particles 45 μm and less in the initial part of the research and particles 10 μm or less for the remainder of the research) were used than even greater densities could be attained as the potential for forming large agglomerates around the larger particles would be reduced. Additionally, during sintering, compression of the compact occurs. The addition of the large $MoSi_2$ particles in the matrix restricts that compression that would normally occur during sintering, thus causing porosity.

Densification (or at least zero open porosity) occurred at 1300°C for pure mullite.[14] In the mullite-$MoSi_2$ system, densification occurred at 1320°C at which point there was zero or negligible open porosity with no conversion to mullite. At this point hot isostatic pressing (HIP'ing) was tried to further compact the body. After densification, samples were HIP'ed at 207 MPa (30 ksi) at 1300-1320 °C. The samples did densify further (an increase on the order of 7%) but when pressureless sintered, the samples displayed de-densification. The de-densification that took place was so great that the final mullite-$MoSi_2$ composite density was lower than if pressureless sintered directly to 1500°C. Since a viscous phase (silica) was present during HIP'ing, it is conjectured that argon (HIP'ing atmosphere) could have infiltrated the viscous phase and been trapped during cooling.

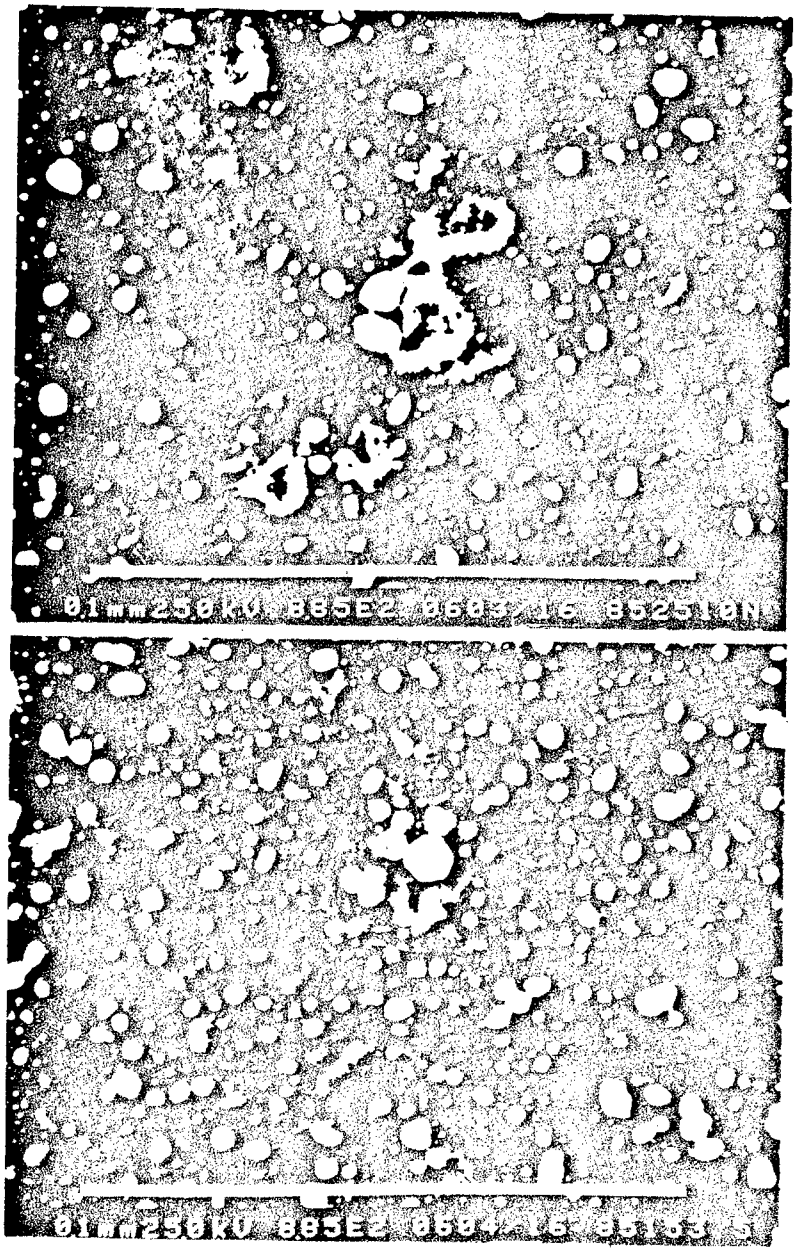

Figure 4.5 15 vol% $MoSi_2$ composite: top -- pH 10, bottom -- pH 3.5

During final sintering, the trapped argon was released causing lower final densities then when pressureless sintered directly. Further attempts to HIP the densified pre-mullitized compact could be made, but the compact should be "canned" (placed within an impervious compressible container that is stable at high temperatures -- much like placing a sample in the evacuated latex bag during CIP'ing -- to prevent contamination). Since densification was hindered by HIP'ing, that processing route was discontinued.

Normal hot pressing procedures for mullite matrix composites attain >97% of theoretical density by hot pressing at temperatures higher than 1600°C and at pressures around 33 MPa. Using the dried alumina-silica-$MoSi_2$ powder, densities of >97% of theoretical were achieved pressing at 1500°C using a pressure of 23 MPa. Figure 4.6 shows the comparison of hot pressed densities to pressureless sintered densities. Recordings of temperature and compaction were taken beginning with the onset of the applied pressure (~1000°C) and ending when the pressure was released during the hot press cycle. For the alumina-silica-$MoSi_2$ powder, compaction took place from when the pressure was applied until mullitization occurred at which time an expansion took place. The general trend was to compact with increasing temperature and pressure (analogous to the transient viscous phase densification of the pressureless sintered bodies) until between 1476° and 1500°C. At these temperatures and the applied 23 MPa pressure, expansion occurred signifying the mullitization of the alumina-silica powder. Since the rule of mixtures density of α-alumina, γ-alumina and silica is 3.48 g/cc, while the density of mullite is 3.16 g/cc, the expansion that occurred during mullitization was because of this density change. The calculated density ratio of alumina-silica to mullite is 1.10 and the ratio of the measured volume change (assuming the weight remains constant) during expansion in the hot press was also 1.10. This expansion (mullitization) took anywhere from 4 to 14 minutes.

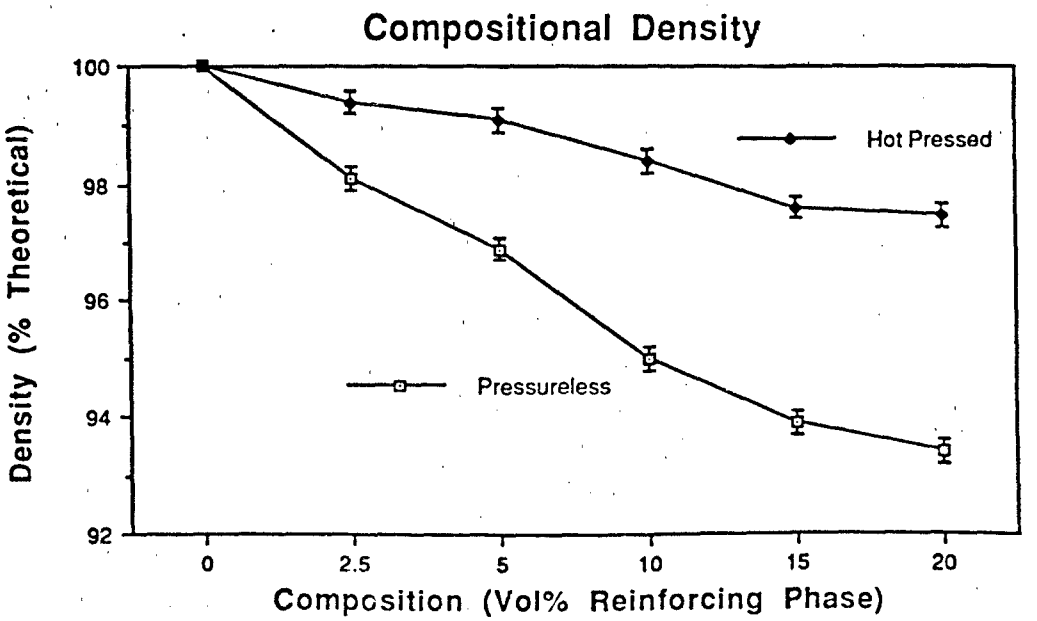

Figure 4.6 Comparison of densities of hot pressed and pressureless sintered samples.

4.3 OXIDATION BEHAVIOR

The oxidation behavior of monolithic $MoSi_2$ is well known[45], but the oxidation characteristics of $MoSi_2$ particles used as a reinforcing phase in a mullite matrix is less well known. Borom, et al.[4] performed oxidation tests on a hot pressed mullite $MoSi_2$ sample and reported a parabolic weight gain for six hours followed by weight loss. To further understand the oxidation process composite samples of 10 and 20 vol% were oxidized at 1400°C. Figures 4.7, 4.8, 4.9 and 4.10 show the 10 vol% sample in the as sintered state, and oxidized for 6, 24 and 48 hours. Figure 4.11 shows the 20 vol% sample after oxidation for 96 hours. Note the continued growth of the protective amorphous silica coating on the $MoSi_2$ particles. The amorphous silica coating grows on $MoSi_2$ particles, then grows together forming over a larger area, until, as seen in the 20 vol% sample silica coats the surface and grows in nodules.

Measurements taken in the as sintered state, after 48 hours of oxidation and after 96 hours of oxidation show that weight gain seems to have leveled off after 96 hours. Additionally the linear dimensional change (calculated based on a starting width of ~0.25 cm) continues to grow but seems also to be leveling off (see Figure 4.12). Conjecture is that the silica layer will continue to grow until all of the surface silicon of the $MoSi_2$ particles is converted to silica. The continued linear dimensional changes can not necessarily be attributed to a volume change, but rather to the continued growth of the silica nodules. Additionally, the silica coating on the particles may not be totally impervious so that there may be some volatilization of the molybdenum as MoO_3. This volatilization would help explain the continued growth of the silica nodules with no further gain in weight, however, the volatilization would seem unlikely. Once the silica layer is formed on the surface of bulk $MoSi_2$ at high temperatures, the formation of Mo_5Si_3 is

Figure 4.7 10 vol% $MoSi_2$ composite, as sintered

Figure 4.8 10 vol% $MoSi_2$ composite oxidized 6 hours

Figure 4.9 10 vol% $MoSi_2$ composite oxidized 24 hours

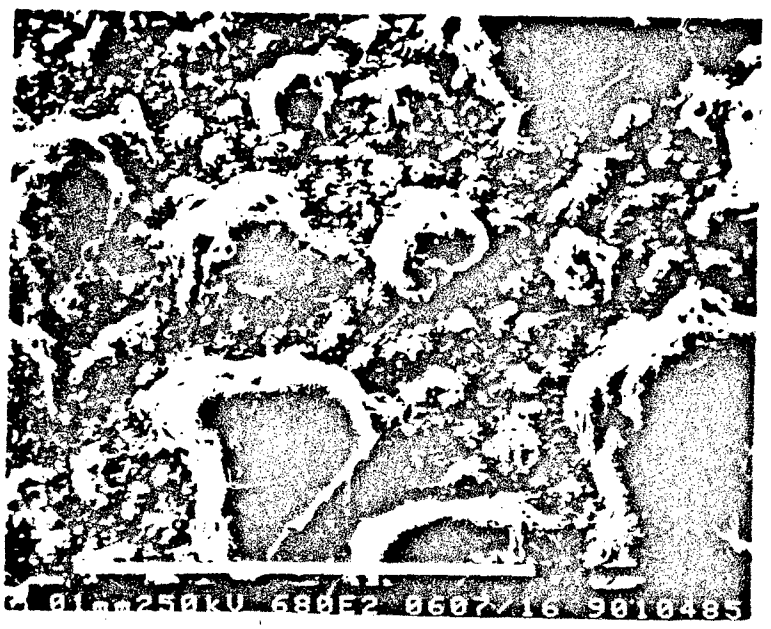

Figure 4.10 10 vol% $MoSi_2$ composite oxidized 48 hours

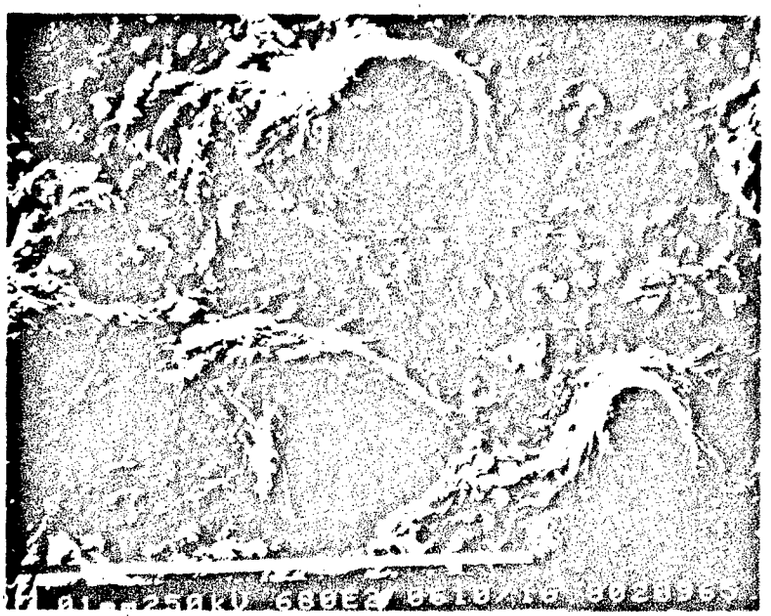

Figure 4.11 20 vol% $MoSi_2$ composite oxidized 96 hours

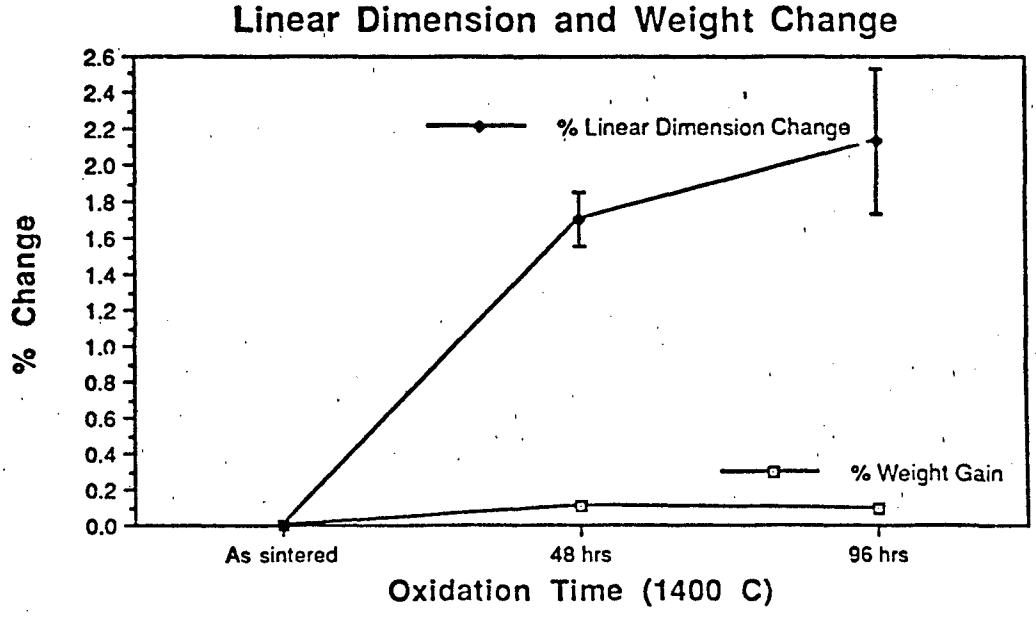

Figure 4.12 Weight and dimensional changes of oxidized 20 vol% $MoSi_2$ composites

favored thermodynamically over the formation of MoO_3.[45] What actually happens to the $MoSi_2$ particles on the surface of the mullite matrix would be a topic of future research to determine why there is continued growth of the silica layer without a corresponding weight gain.

The fact that the silica coating grows on the surface of the $MoSi_2$ is reported in literature[4,44-46,55] although in none of the references is a reason why it grows on the surface other than listing the oxidation reaction that is in Section 2.6. For instance, "Monolithic $MoSi_2$ . . . initially form SiO_2 and Mo-oxides but the latter evaporates leaving a protective SiO_2 film. This film results in usable lives in excess of 2000 hours at 1650°C."[55] It is conjectured that the silica layer grows out of the surface of the $MoSi_2$ due to a volume expansion since the density of silica is 2.2 g/cc while the density of $MoSi_2$ is 6.2 g/cc.

4.4 MECHANICAL PROPERTIES

4.4.1 TOUGHNESS

SENB tests were carried out to determine the fracture toughness (K_{Ic}) of hot pressed samples (2.5, 5, 10 ,15 and 20 vol% $MoSi_2$), (see Section 2.9). Additionally, one hot pressed billet (containing 20 vol% $MoSi_2$) was sliced into nine test bars, each of which were notched. Three were tested in the as sintered state, three were tested after oxidation for 48 hours at 1400°C, and three were tested after oxidation for 96 hours at 1400°C.

K_{Ic} values reported in literature for mullite are generally around 2.2. Pure mullite samples made by the pressureless sintering technique previously discussed averaged a K_{Ic} value of 2.03. These lower K_{Ic} values may be caused by excess silica formed at the grain boundaries -- TEM analysis would confirm or deny this supposition. Figure 4.13 shows the comparison of the various mullite - $MoSi_2$ K_{Ic} values along with that of pure mullite

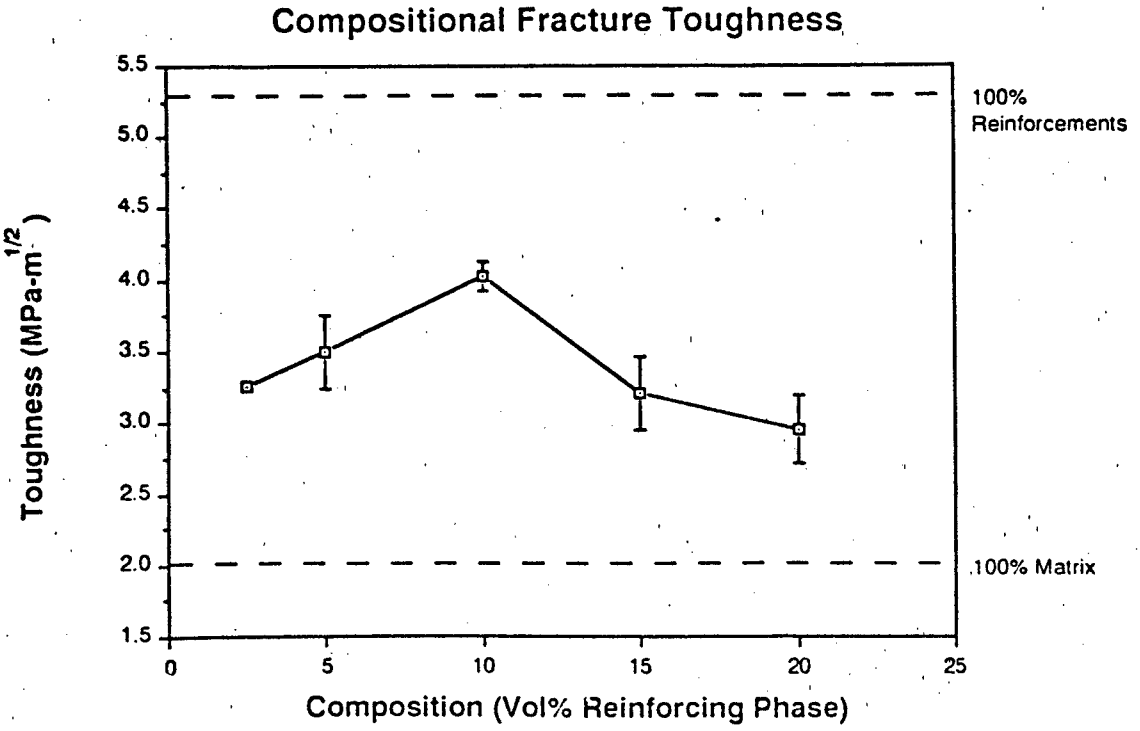

Figure 4.13 Fracture toughness (K_{Ic}, MPa·m$^{1/2}$) as a function of composite composition

and pure $MoSi_2$.[47] K_{Ic} values increase until they reach a maximum at 10 vol% $MoSi_2$ particles and then the K_{Ic} values declines but still stays above the K_{Ic} value of monolithic mullite.

Figures 4.14, 4.15, and 4.16 show the crack path caused by a microindenter. As can be seen in the progressively higher magnification of the 20 vol% $MoSi_2$ reinforced sample, the crack path wends its way around $MoSi_2$ particles. The explanations for this crack behavior are: (1) cracks are deflected around particles in hydrostatic tension[23] (see Figure 2.12), since $MoSi_2$ has a higher coefficient of thermal expansion than mullite, the $MoSi_2$ particles are in tension after cooling, (2) $MoSi_2$ has a K_{Ic} value 2.5 times that of mullite so that the crack follows the path of least resistance -- through the mullite and around the $MoSi_2$ particles, and/or (3) if a glassy phase is present at the particle-matrix interface, then the crack would rather go through the weaker/less tough glassy phase then through the mullite matrix or the $MoSi_2$ particles.

Of the various toughening mechanisms listed in Chapter 2, it would seem that crack deflection is the major toughening mechanism. $MoSi_2$ has a higher coefficient of thermal expansion (see Figure 4.17) than mullite so, upon cooling from processing temperatures, the particles are in tension while the matrix is in compression which results in higher toughness. This toughening is most effective at the 10 vol% $MoSi_2$ loading and decreases with the higher $MoSi_2$ loadings due to too more and more of the composite in tension (more $MoSi_2$ particles added) due to cooling. Additionally, if the glassy phase is present at the particle-matrix interface, the more particles being added would result in more of the glassy phase being present in the composite which would reduce fracture toughness. Another toughening mechanism that could be applicable is crack impediment which is demonstrated by the crack from the microindenter having to go around the $MoSi_2$ particles and eventually stopping at a particle.

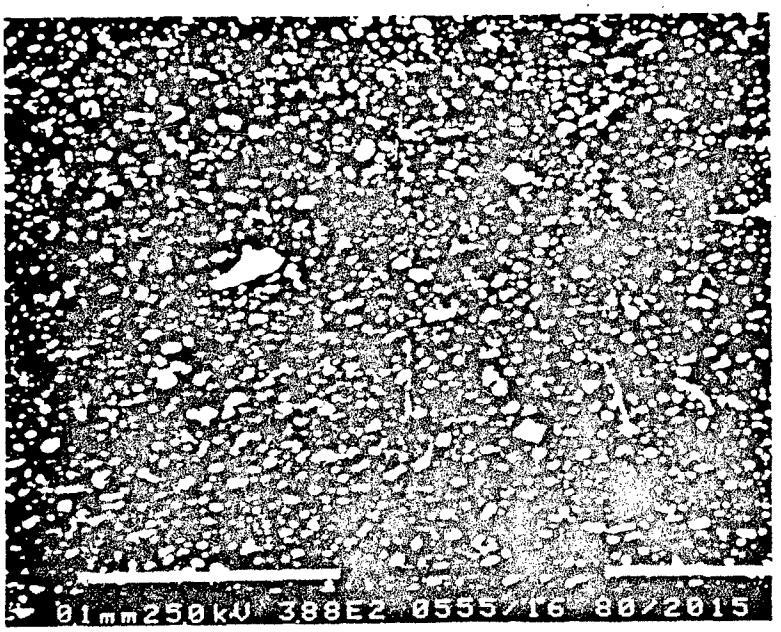

Figure 4.14 Crack caused by 3 kg load microindenter

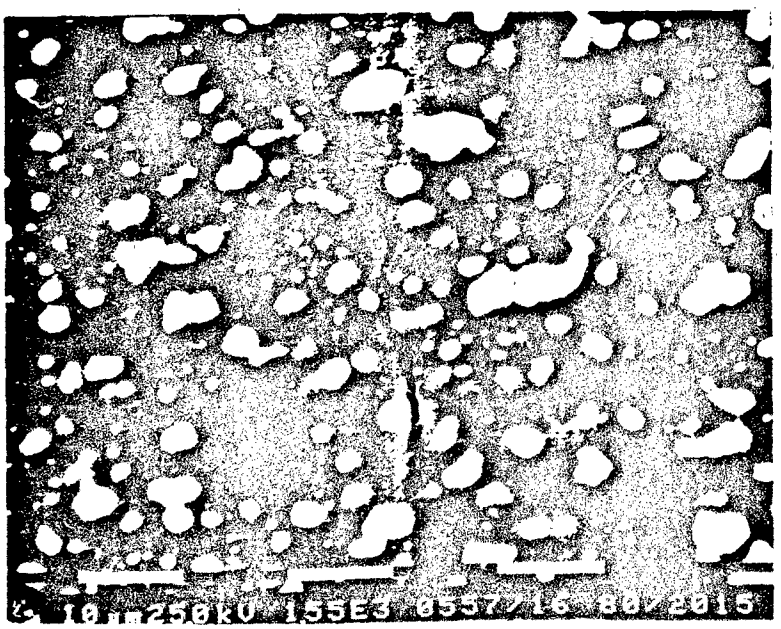

Figure 4.15 Particle - matrix interactions caused by the crack

Figure 4.16 Crack path around a particle.

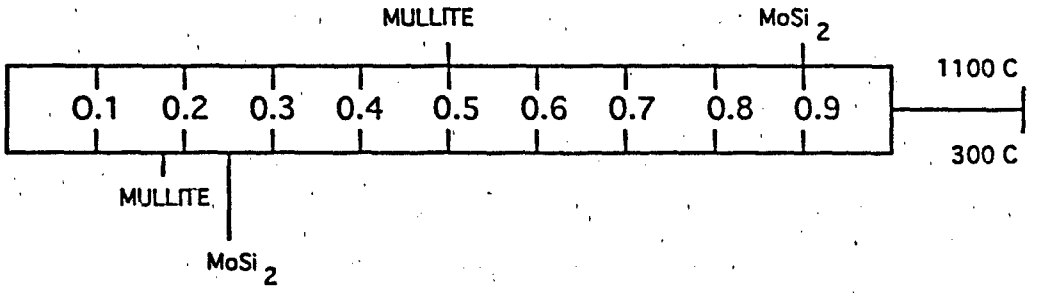

Figure 4.17 Comparison of % linear expansion of mullite and $MoSi_2$ at 300°C and 1100°C

When oxidized, the silicon from the $MoSi_2$ forms the protective amorphous silica layer, as discussed earlier. This seems to provide a healing effect to the material giving it greater toughness. Figure 4.18 shows the apparent toughening trend with increasing oxidation, with the as sintered sample much lower in fracture toughness than the oxidized samples. Figures 4.19 and 4.20 show the fracture surfaces of one of the as sintered samples and one of the samples oxidized for 96 hours. The comparison is startling. In the as sintered surface, crack origins can easily be seen, however, in the oxidized sample, it is difficult to determine where the fracture initiated. (Note, $MoSi_2$ particles are 10 μm or less, monoliths on the surface are dust or other artifacts that were on the surface when sputter coated with gold-palladium.) What occurs is that the protective silica layer grows over the crack region (not into the region) sealing it off. The end result is a self-healing material -- any cracks or flaws in the surface can be healed during high temperature use. (The fact that the required atomically sharp crack caused by notching is "healed" during oxidation results in artificially high fracture toughness (apparent toughness) values. So while the measured values may not be totally correct, they do demonstrate the "healing" effect of oxidation.)

Although no high temperature testing was accomplished as part of this study, it can be assumed that the toughness would continue to increase after the $MoSi_2$ had passed its brittle to ductile transition (~1000°C). At this point the $MoSi_2$ particles would act as ductile particle ligaments in the matrix and toughness would increase by the mechanisms stated earlier along with the primary contribution coming from crack impediment. The proposed glassy interface between the $MoSi_2$ particles and the matrix would probably provide for a decrease in toughness at high temperatures due to its lowered viscosity.

If future research shows that there is indeed a glassy interface between the $MoSi_2$ particles and the mullite matrix, then a key to future use of this composite is to minimize or eliminate that glassy phase. One way to accomplish this is through better processing -- add

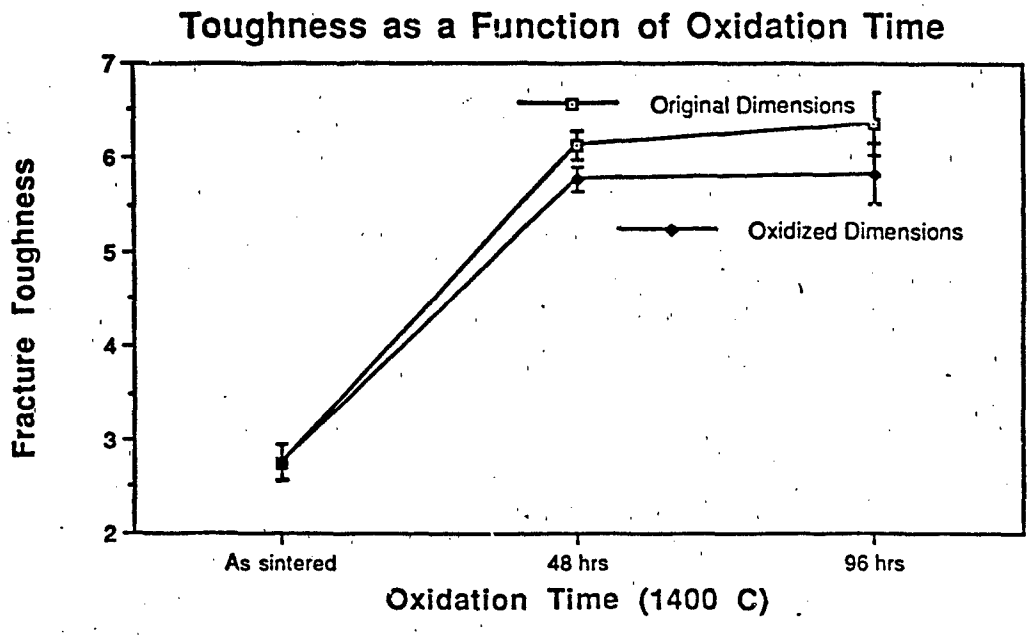

Figure 4.18 Apparent toughness (K_{Ic}, MPa·m$^{1/2}$) as a factor of oxidation time for samples original dimensions and for the samples oxidized dimensions (note that the notches for SENB testing were cut prior to oxidation)

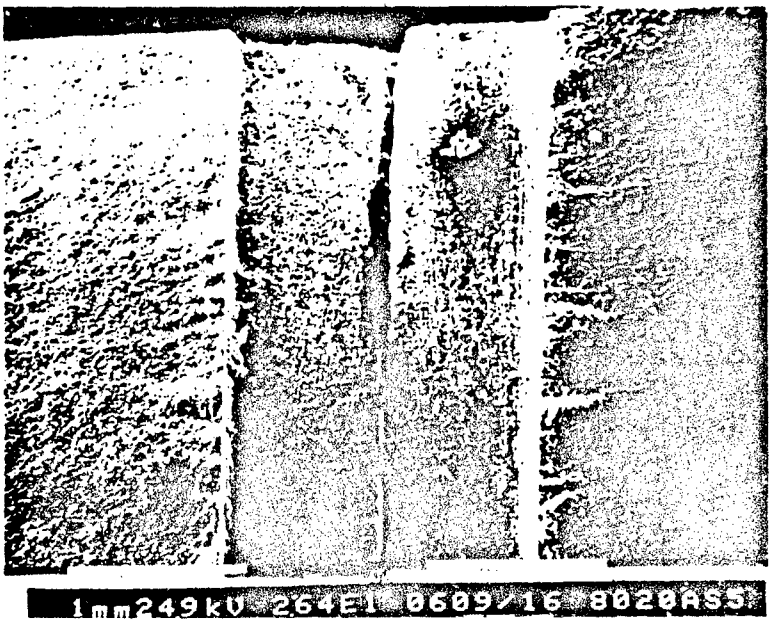

Figure 4.19 Fracture surface of a 20 vol% $MoSi_2$ composite -- as sintered

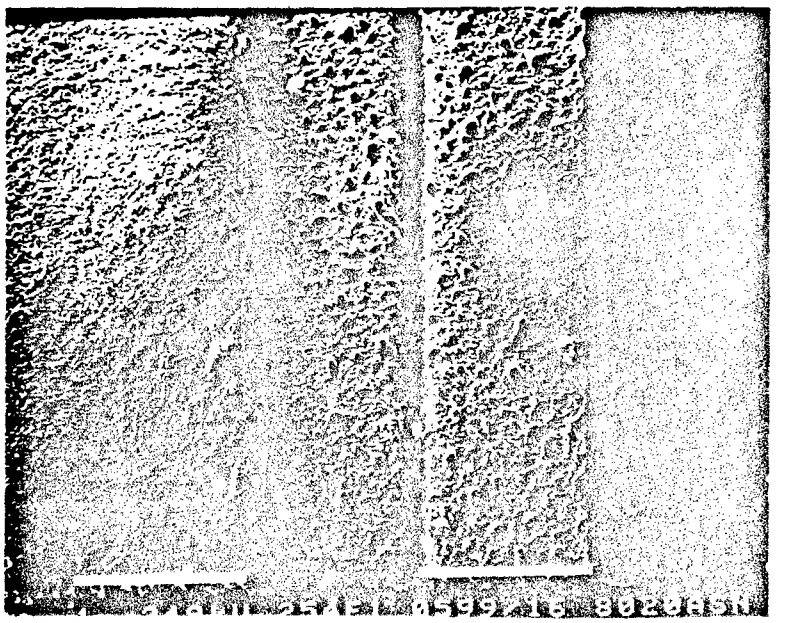

Figure 4.20 Fracture surface of a 20 vol% $MoSi_2$ composite -- oxidized 96 hours

a greater amount of alumina than called for in stoichiometric mullite so that the extra alumina will react with the unwanted silica during sintering to form mullite.

4.4.2 STRENGTH

Strength tests were conducted similarly to the toughness tests. Measurements were taken from hot pressed 2.5, 5, 10, 15 and 20 vol% $MoSi_2$ samples, pure mullite samples and a 20 vol% $MoSi_2$ hot pressed sample cut into nine test specimens with the tensile face of each polished to 0.3 μm. Three each were then tested as sintered, three were oxidized at 1400°C for 48 hours and tested, and three were tested after oxidizing for 96 hours at 1400°C.

Figure 4.21 shows the comparison of the unoxidized room temperature strength of the various compositions of mullite and $MoSi_2$, pure mullite, and pure $MoSi_2$. It is interesting to note that until approximately 15 vol% $MoSi_2$ is added, the strength of the composite is less than that of the matrix. What this suggests is that there is a critical amount of $MoSi_2$ that needs to be added before any strengthening is achieved and that until that critical volume fraction is reached, the mullite matrix perceives the particulate inclusions as flaws or pores which reduce strength. When more than the critical amount of $MoSi_2$ is added, then a synergistic effect is attained, as the composite strength is greater than the strength of either of its monolithic constituents.

After oxidation (even with the weight gain and dimensional growth) the strength shows a general upward trend with increasing strength as oxidation time is increased (see Figure 4.22). Again this, along with the toughening, is causes by the protective silica layer which grows on the surface of the $MoSi_2$ particles providing a healing of the surface flaws of the sample, thus increasing its strength.

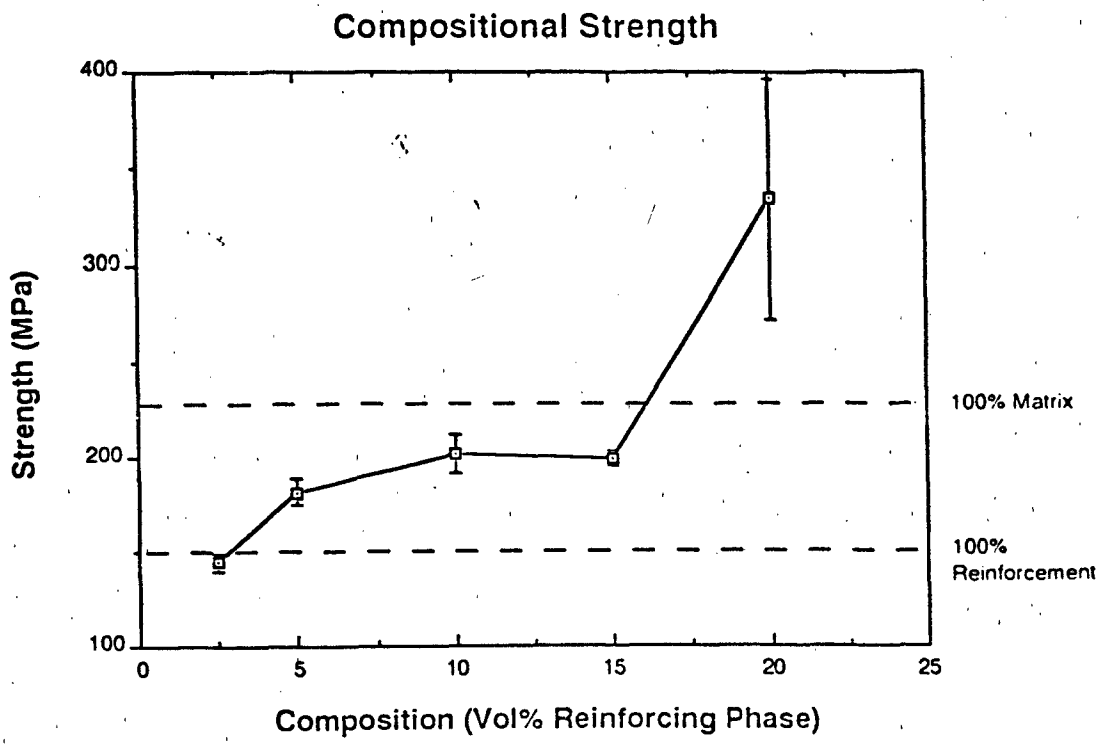

Figure 4.21 Strength as a function of composite composition

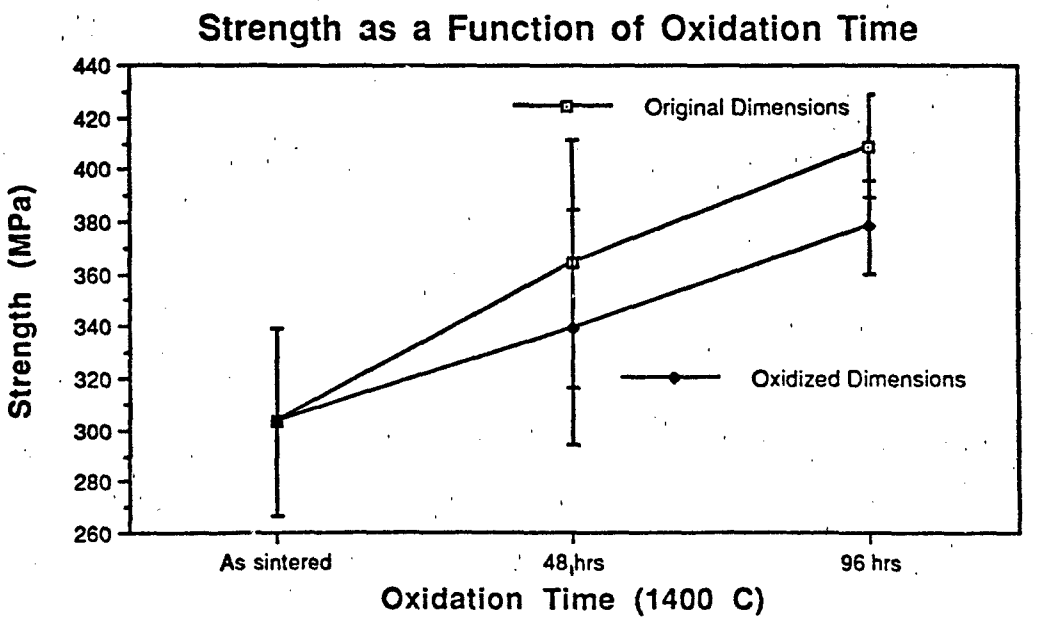

Figure 4.22 Strength of 20 vol% $MoSi_2$ composite as a function of oxidation time

It is interesting to note that with increasing $MoSi_2$ particles added to the composite (above 10 vol%), strength improves and fracture toughness declines. Although no reason or hypothesis will be presented here, this trend has been reported in other composite systems suggesting that in many composite systems there is a trade-off -- improve fracture toughness at the expense of strength, or improve strength at the expense of fracture toughness. In self reinforced Si_3N_4 grain size plays a key role in fracture toughness. At small grain sizes, the material has a K_{Ic} of 5.5 $MPa \cdot m^{1/2}$ with a corresponding strength of 1170 MPa. At larger grain sizes, the material has a higher value of K_{Ic} of 11 $MPa \cdot m^{1/2}$ but a lower strength of 790 MPa.[25] In a 5 vol% mullite whisker reinforced mullite matrix composite, K_{Ic} = 1.8 $MPa \cdot m^{1/2}$ and σ = 430 MPa. At 10 vol% mullite whiskers, K_{Ic} = 2.6 $MPa \cdot m^{1/2}$ and σ = 415 MPa.[42] Additionally, in a zirconia-mullite composite, K_{Ic} = 4.4 $MPa \cdot m^{1/2}$ and σ = 350 MPa. Adding CaO to that zirconia-mullite composite increases K_{Ic} to 4.9 $MPa \cdot m^{1/2}$ yet strength goes down to 200 MPa.[56]

CHAPTER 5
CONCLUSIONS

- Mullite and $MoSi_2$ are phase compatible and stable as determined by x-ray diffraction and SEM analysis.

- The composite can be hot pressed to higher densities at a lower temperature and pressure (1500°C, 23 MPa) than is usually used for mullite based composites because of the use of the mullite precursor powder (alumina coated with silica).

- The composite can be processed to good densities (>93% of theoretical for up to 20 vol% $MoSi_2$) however, further refinement of the process is required to attain full density.

- Room temperature toughness of the mullite matrix is improved to a K_{Ic} value of between 3 and 4 $MPa \cdot m^{1/2}$ depending upon the amount of $MoSi_2$ added.

- Room temperature strength of the mullite matrix is improved with additions of more than the critical volume fraction (~15 vol%) of $MoSi_2$ from 230 MPa for pure mullite up to a maximum measured strength of 420 MPa (for 20 vol% addition of $MoSi_2$).

- The material is self healing -- with increases in fracture toughness and strength after oxidation. The protective silica layer forms over cracks and flaws thus healing them and imparting improved mechanical properties to the composite.

- A mullite matrix, $MoSi_2$ particle reinforced system has good room temperature properties, and excellent oxidation characteristics. Further research is warranted to fully investigate this composite for use as a high temperature material.

CHAPTER 6

FUTURE RESEARCH

The work presented in this thesis has focused mainly on proving that a mullite - $MoSi_2$ composite is viable at low temperatures, and that pressureless sintering techniques could be used to fabricate the composite. In order to further verify that the composite is a useful one for high temperature use and to improve on the pressureless sintering densities, the following work should be accomplished:

a. Further refine the pressureless sintering process so that fully dense composites can be fabricated. Areas in which to explore are: constituent particle size, the role different pH's can play, variations on the colloidal processing technique itself (proportions of constituents, type of constituents, etc.), and determine how much extra alumina to add to convert the proposed glassy phase that exists at the particle-matrix interface.

b. Perform extensive oxidation studies -- oxidize for prolonged periods of time at different temperatures and study weight change, dimensional change, growth of the silica layer, etc. Also, investigate the effects that temperature cycling will have because, if this composite is to be used at high temperatures in aerospace applications, then it must be able to withstand the rigors of low to high temperature cycling.

c. Conduct high temperature strength, fracture toughness and creep testing of the composite at a variety of temperatures, after different soak times, and after thermal cycling.

d. Investigate the de-densification phenomenon discovered when HIP'ing was attempted. Through use of a different technique (e.g. "canning" the sample), HIP'ing could be a viable densification aid. Further, information learned from this de-densification

may enable the researcher to attain better pressureless sintered densities without the aid of the HIP.

e. Perform characterization studies on the as sintered and oxidized composites. Investigate: the protective silica layer and how it interacts with the mullite matrix, the interface between the $MoSi_2$ particle and the mullite matrix (this could help determine the volume fraction of the constituents to be used for processing for better mechanical properties), high temperature failure mechanisms and high temperature toughening mechanisms.

f. Determine the optimum volume fraction of $MoSi_2$ to be dispersed in the mullite matrix for optimal mechanical properties. This would entail investigating a wide realm of volume fractions of $MoSi_2$ and then performing the low and high temperature testing of the promising composites.

BIBLIOGRAPHY

1. N.D. Corbin, G.A. Rossi, P.M. Stephan, "Making Ceramics Tougher," *Machine Design*, pp. 84-89, July 23, 1987.

2. J. Schlichting, "Molybdenum Disilicide as Component of Modern High Temperature Composites," *High Temp. - High Pressures*, **10**, 241-269, (1978).

3. Notes and Discussions with I.A. Aksay.

4. M.P. Borom, M.K. Brun, L.E. Szala, "Kinetics of Oxidation of Carbide and Silicide Dispersed Phases in Oxide Matrices," *Adv. Ceram. Mat.*, **3** [5] 491-497 (1988).

5. R.J. Hunter, Foundations of Colloid Science Volume I, Clarendon Press, Oxford (1986).

6. D.J. Shaw, Introduction to Colloid and Surface Chemistry, Third Edition, Butterworths (1980).

7. H.C. Hamaker, *Physica*, **4** 1058 (1937).

8. S. Usui, "Heterocoagulation" in Progress in Surface and Membrane Science; Edited by J.F. Danielli, M.D. Rosenberg, and D.A. Cadenhead, **5** 223-226 (1972).

9. C.S. Hirtzer and R. Rajogopalan, Advanced Topics in Colloidal Phenomena, Noys Publications, New Jersey (1985).

10. I. A. Aksay and R. Kikuchi in Science of Ceramic Chemical Processing; Edited by L.L. Hench and D.R. Ulrich, Wiley, New York (1986).

11. W.C. Hasz, Master's Thesis, Massachusetts Institute of Technology (1983).

12. R.M. Allman, Master's Thesis, University of California at Los Angeles (1983).

13. J. Cesarano,III, Master's Thesis, University of Washington (1988).

14. J.E. Webb, Master's Thesis, University of Washington (1991).

15. T.W. Healy, G.R. Wiese, D.E. Yates and B.B. Kavanaga, "Heterocoagulation in Mixed Oxide Colloidal Dispersions," *J. Colloid. Interface Sci.*, **42** [3] 647-49 (1973).

16. F.F. Lange and K.T. Miller, "Pressure Filtration Consolidation Kinetics and Mechanics," *Am. Ceram. Soc. Bull.*, **66** [10] 1498-1504 (1987).

17. J. Dodds and M. Leitzelement, "The Relation Between the Structure of Packing Particles and Their Properties," in Physics of Finely Divided Matter, Edited by N. Boccara and M. Daoud (1985).

18. T.J. Fennely and J.S. Reed, "Mechanics of Pressure Casting," *J. Am. Ceram. Soc.*, **55** [5] (1972).

19. R.W. Rice, "Ceramic Matrix Composite Toughening Mechanisms: An Update," *Ceram. Eng. Sci. Proc.*, **6** [7-8] 589-607 (1985).

20. G.E. Dieter, Mechanical Metallurgy, McGraw-Hill (1986) pp. 246-250.

21. I.J. McColm, Ceramic Science for Materials Technologists, Leonard Hill, Scotland (1983) pp. 123-125.

22. S.T. Buljan, A.E. Pasto and H.J. Kim, "Ceramic Whisker- and Particulate-Composites: Properties, Reliability and Applications," *Ceramic Bulletin*, **68** [2]2 387-94 (1989).

23. R.W. Rice, "Mechanisms of Toughening in Ceramic Matrix Composites," *Ceram. Eng. Sci. Proc.*, **2** [7-8] 589-607 (1981).

24. M. Taya, S. Hayashi, A.S. Kobayashi, and H.S. Yoon, "Toughening of a Particulate - Reinforced Ceramic Matrix Composite by Thermal Stress," *J. Am. Ceram. Soc.*, **73** [5]5 1382-91 (1990).

25. P.F. Becher, "Microstructural Design of Toughened Ceramics," *J. Am. Ceram. Soc.*, **74** [2] 2 255-269 (1991).

26. D.J. Green, R.H.J. Hannick and M.V. Swain, Transformation Toughening of Ceramics, CRC Press Inc. (1989).

27. I.J. McColm, Ceramic Hardness, Plenum Press, New York (1990).

28. W.D. Kingery, H.K. Bowen, D.R. Uhlmann, Introduction to Ceramics, 2nd Edition, John Wiley and Sons, New YHork (1975).

29. J.S. Reed, Introduction to the Principles of Ceramic Processing, John Wiley and Sons, New York (1988).

30. I.A. Aksay and J.A. Pask, "The Silica-Alumina System: Stable and Metastable Equilibria at 1.0 Atmosphere," *Science*, 183 pp 69-71 (1974).

31. D.A. Lessing, R.S. Gordon, and K.S. Mazdiyasni, "Creep of Polycrystalline Mullite," *J. Am. Ceram. Soc.*, **66** [12] 874-880 (1983)

32. I.A. Aksay, D.M. Dabbs, and M. Sarikaya, "Mullite for Structural, Electronic and Optical Applications," *J. Am. Ceram. Soc.*, **74** [10] 2343-58 (1991).

33. A.D. Hynes and R.H. Doremus, "High-Temperature Compressive Creep of Polycrystalline Mullite," *J. Am. Ceram. Soc.*, **74** [10] 2469-75 (1991).

34. M.D. Sacks, H.W. Lee and J.A. Pask, "A Review of Powder Preparation Methods and Densification Procedures for Fabricating High Density Mullite," pp 167-207, in Mullite and Mullite Matrix Composites, Ceramic Transactions Vol. 6, Edited by S. Somiya, R.F. Davis and J.A. Pask. The American Ceramic Society, Westerville Oh, (1990).

35. T.I. Mah, and K.S. Mazdiyasni, "Mechanical Properties of Mullite," *J. Am. Ceram. Soc.*, **66** [10] 699-703 (1983).

36. S Kanzaki, H. Tabata, T. Kumazawa, and S. Ohta, "Sintering and Mechanical Properties of Stoichiometric Mullite," *J. Am. Ceram. Soc.*, **68** [1] C-6 - C-7 (1985).

37. M.G.M.U. Ismail, Z. Nakai and S. Somiya, "Microstructure and Mechanical Properties of Mullite Prepared by the Sol-Gel Method," *J. Am. Ceram. Soc.*, **70** [1] C-7 - C-8 (1987).

38. M.G.M.U. Ismail, Z. Naikai, and K. Minegishi, "Synthesis of Mullite Powder and Its Characteristics," *Int. J. High Technol. Ceram.*, **2** [2] 123-24 (1986).

39. P.C. Dokko, J.A. Pask and K.S. Mazdiyasni, "High Temperature Mechanical Properties of Mullite Under Compression," *J. Am. Ceram. Soc.*, **60** [3-4] 150-155 (1977).

40. R.F. Davis, I.A. Aksay, and J.A. Pask, "Decomposition of Mullite," J. *Am. Ceram. Soc.*, **55** [2] 98-101 (1972).

41. M.D. Sacks and J.A. Pask, "Decomposition of Mullite," *J. Am. Ceram. Soc.*, **55** [2] 98-101 (1972).

42. Ceramic Transactions, Vol. 6, Mullite and Mullite Matrix Composites, Edited by S. Somiya, R.F. Davis and J.A. Pask, American Ceramic Society, Westerville, OH 1990.

43. M.D. Sacks, G.W. Scheiffele, N. Bozkurt and A. Ulicny, "Fabrication of Mullite and Mullite Based Composites by Transient Viscous Sintering of Composite Powders," presented at the 93d National Meeting of the American Ceramic Society, Westerville, OH (1990).

44. E.W. Lee, J. Cook, A. Khan R. Mahåpatra and J. Waldman, "The Oxidation Resistance of $MoSi_2$ Composites," *Journal of Materials*, pp 54-57, March 1991.

45. C.D. Wirkus and D.R. Wilder, "High Temperature Oxidation of Molybdenum Disilicide," *J. Am. Ceram. Soc.*, **49** [4] 173-177 (1966).

46. V. Bizzarri, B. Lindor, and N. Lindskog, "Molybdenum Disilicide Heating Elements: Meeting Advanced Ceramics Requirements," *Ceramic Bulletin*, **68** [10] 1834-1841 (1989).

47. J.J. Petrovic and R.E. Honnell, "$MoSi_2$ Particle Reinforced SiC and Si_3N_4 Matrix Composites," unpublished report.

48. J.J. Petrovic, R.E. Honnell, T.E. Mitchell, R.E. Wade, and K.J. McClellan, "ZrO_2 Reinforced - $MoSi_2$ Matrix Composites," to appear in Proceedings of the 15th Annual Conference on Composites and Advanced Ceramics, Cocoa Beach, FL, American Ceramic Society, Westerville, OH.

49. J.J. Petrovic and R.E. Honnell, "SiC Reinforced - $MoSi_2/WSi_2$ Alloy Matrix Composites," *Ceram. Eng. Sci. Proc.*, **11**, 734 (1990).

50. R.W. Davidge, Mechanical Behavior of Ceramics, Cambridge University Press (1979).

51. Binary Alloy Phase Diagrams, 2nd Edition, Volume 3, Edited by T.B. Massalski, ASM International, OH.

52. B.J. Tarasevich, Masters Thesis, University of Washington.

53. ASTM Designation: C20-87, Standard Test Methods for Apparent Porosity, Water Absorption, Apparent Specific Gravity and Bulk Density of Burned Refractory Brick and Shapes by Evacuation.

54. ASTM Designation: E399-74, Standard Method of Test for Plain-Strain Fracture Toughness of Metallic Materials.

55. E.A. Gulbransen and G.H. Meier, "Thermochemical Stability Diagrams for Condensed Phases and Tabulation of Volatile Species Over Condensed Phases for Thirteen Metal-Oxygen-Silicon Systems at 1000 and 1250 K," Final Report - Volume II, Prepared for: DOE Fossil Energy Materials Program, Oak Ridge National Laboratory, Oak Ridge, TN, May (1988).

56. J.S. Moya, "Reaction Sintered Mullite-Zirconia and Mullite Zirconia-SiC Ceramics," pp 495-507, in Mullite and Mullite Matrix Composites, Ceramic Transactions Vol. 6, Edited by S. Somiya, R.F. Davis and J.A. Pask. The American Ceramic Society, Westerville Oh, (1990).